IITRI

IITRI Report No. C6186-5
(Final Report)

DEVELOPMENT OF PARTICULATE EMISSIONS
CONTROL TECHNIQUES
FOR SPARK IGNITION ENGINES

Environmental Protection Agency
Air Pollution Control Office
Division of Motor Vehicle R & D
Ann Arbor, Michigan   48103

IIT RESEARCH INSTITUTE

IITRI Report No. C6186-5
(Final Report)

DEVELOPMENT OF PARTICULATE EMISSIONS CONTROL
TECHNIQUES FOR SPARK IGNITION ENGINES

June 22, 1969 to November 30, 1970

Prepared by

Sudesh K. Sood

and

Richard Karuhn

Submitted by

IIT Research Institute
10 West 35 Street
Chicago, Illinois   60616

for

Environmental Protection Agency
Air Pollution Control Office
Division of Motor Vehicle R & D
Ann Arbor, Michigan   48103

Attention: Mr. Charles Gray, Jr.
Project Officer
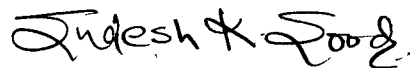

February, 1971

Copy No._____

IIT RESEARCH INSTITUTE

ii

FOREWORD

This is the Final Report on IITRI Project C6186, entitled, "Development of Particulate Emissions Control Techniques for Spark Ignition Engines." The research program was sponsored by the Air Pollution Control Office (formerly the National Air Pollution Control Administration) of the Environmental Protection Agency under Contract No. CPA-22-69-134. Personnel contributing to the project were Ted Rymarz, Don Werle, Brent Boldt, Henry Karplus, John Stockham and Meryl Jackson.

This report covers the period from June 22, 1969 to November 30, 1970. All data are recorded in IITRI Logbooks C19521, C19678 and C20199.

Respectfully submitted,
IIT Research Institute

Sudesh K. Sood
Associate Engineer

Richard Karuhn
Experimentalist

Approved by:

John Stockham
Manager, Fine Particles
Research

SKS:db

ABSTRACT

DEVELOPMENT OF PARTICULATE EMISSIONS CONTROL
TECHNIQUES FOR SPARK IGNITION ENGINES

This report describes the experimental results of two techniques for the removal of particulate contaminants from spark ignition engine exhausts.

The first technique was based on the thermal deposition of lead aerosol particles in the size range $0.1 - 0.8\mu$ in a packed bed. The effect of gas-packing temperature differential, packing material, packing shape and size, contamination build-up, and gas velocity on collection efficiency of the bed was studied. Experimental results show that collection efficiency of the packed bed device depends primarily on the gas-packing temperature differential. At a gas velocity of 15.5 cm/sec the collection efficiency of the device exceeds 95% at temperature differential greater than 200°C. Increasing the gas velocity to 130 cm/sec lowered the collection efficiency of the bed by 10-15%.

The second technique was based on the use of sonic waves to increase the collisions between the aerosol particles and the relatively coarse particles of a fluidized bed, and hence increase the collection efficiency. The effect of sound frequency, gas velocity, and power input to the sound driver units was studied. Experimental results showed that there was no significant effect of sound frequency, in the range 250-2700 HZ, on collection efficiency of the fluidized bed. Collection efficiency of the fluidized bed was found to increase sharply with power input to the sound driver units when standing sound waves were used. The use of travelling sound waves did not enhance the collection efficiency of the fluidized bed significantly.

TABLE OF CONTENTS

IIT RESEARCH INSTITUTE

TABLE OF CONTENTS (Cont'd)

LIST OF FIGURES

IIT RESEARCH INSTITUTE

vii

LIST OF TABLES

IIT RESEARCH INSTITUTE

DEVELOPMENT OF PARTICULATE EMISSIONS CONTROL
TECHNIQUES FOR SPARK IGNITION ENGINES

I. INTRODUCTION

The operation of millions of motor vehicles in the United States produces significant exhaust particulate emissions. The majority of the current motor vehicles operate with fuel containing lead antiknock compounds; these vehicles emit exhaust particulates containing lead. Vehicles burning gasoline containing 3 ml of TEL (Tetra Ethyl Lead) motor mix per gallon have been observed to emit from 1 to 500 μg of lead compounds per liter of exhaust. It is also estimated that these vehicles emit about 0.1-0.2 grams per mile of lead compounds. The concentration of lead compounds in the exhaust gas depends on the operating speed of the car (Ref. 1,2). The size of lead bearing particulates in automobile exhausts has been found to be less than 1 μ by many investigators (Ref. 3,4,5). The exhaust flow in vehicle exhaust systems ranges from about 9 to 95 standard liters per second (approximately 20 to 200 scfm), while the exhaust gas temperature depends on position in the exhaust system and engine operating conditions and can range from 150 to 1000°C (Ref. 6). Automotive exhaust particulates containing lead compounds have also been reported to cause adverse effects on vegetation, crops and human health (Ref. 7,8,9).

Of the myriad of particulate collection equipment commercially available none are capable of high collection efficiency on submicron sized particles when space and cost limitations imposed by the proposed use are applied. Careful analysis of the problem from a systems engineering approach leads to the conclusion that the potential development of a suitable device is likely to result only from intense technical efforts in a relatively narrow area of technology.

A review of state-of-the-art techniques for particulate removal reveals that the many types of devices available for

removal of particles from gas streams all depend on either one or more of the following principles:

1. Mechanical; filters or screens
2. Inertial forces; centrifuges, cyclones, scrubbers
3. Electrostatic forces; electrostatic precipitators or charged screens
4. Gravitational forces; settling chambers
5. Magnetic forces; magnetic separators
6. Thermal forces; thermal precipitators

The separation of particles from a gas stream implies relative motion between the particles and the gas. Hence, the relative magnitudes of the separating force and the viscous drag on the particles is an important parameter in most separation mechanisms. With large particles, 100 μ in diameter or larger, the mass of the particles is high and the force of gravity can be used to achieve separation in a settling chamber. As particle size decreases, the settling velocity also decreases and other techniques must be employed to achieve separation.

With particles in the size range 5 to 100 μ, the mass to surface area ratio is high enough so that inertial forces can be effectively employed to achieve separation. Cyclones, centrifuges, impactors, and scrubbers are efficient devices in this size range. Although there are differences in these devices, they all depend on the inertia of the aerosol particles. Cyclones direct the gas into a spiral path and achieve separation by the centrifugal force on the particle. Centrifuges differ from cyclones only in that a mechanically driven fan or rotor is used to produce the rotational velocity. Impactors achieve collection by interposing a target in the path of the dirty gas stream, causing those aerosol particles with sufficient inertia to impact on the target. Scrubbers depend upon the inertia of the aerosol particles and the scrubbing droplets to bring about collision and consequent capture of the aerosol particles.

Particles less than 5 μ in diameter have a low mass to drag

ratio. This is easily apparent from Table I which presents the settling velocity of particles in air.

Table I

SETTLING VELOCITY OF 2.0
SPECIFIC GRAVITY PARTICLES IN AIR

Diameter, Microns	Settling Velocity, cm/sec
0.01	1.5×10^{-5}
0.1	1.8×10^{-4}
1.0	7×10^{-3}
5.0	0.2
10.0	0.6
50.0	20
100	45

The problems encountered in attempting to separate 1 μ diameter particles from a gas stream can be illustrated by calculating some of the geometric parameters of a hypothetical centrifugal separator. At low relative velocities the particle will move through the medium at a rate directly proportional to the force acting upon it. Thus, in a centrifugal field, in differential form:

$$\frac{dR}{dt} = V_s F_c \qquad (1)$$

where

R = the radius of curvature of the stream path

V_s = the settling velocity at one gravity of force

F_c = the centrifugal force, gravities

t = time

the centrifugal force, F_c is

$$\frac{V^2}{g_c R} \qquad (2)$$

where g_c is the gravitational constant, V is the linear velocity
and the residence time is

$$\frac{L}{V} \qquad (3)$$

where L is the path length, the integrated relationship is then

$$\Delta R = V_S \frac{V^2}{g_c R} \frac{L}{V} = V_S \frac{VL}{g_c R} \qquad (4)$$

If we assume that a relative motion of one tenth of a foot is
required (equivalent to assuming a stream one-tenth of a foot
in width), a linear velocity of 100 feet per second and a radius,
R, of 0.5 feet then

$$0.1 = \frac{7 \times 10^{-3}}{30.5} \times \frac{100 \, L}{32.2 \times .5}$$

$$L = 70 \text{ ft}$$

That is, a path length of 70 ft would be required or more than
22 revolutions in a one-foot diameter cyclone. This would be
difficult to achieve and would require considerable energy input.
Also, to accomodate 146 cfm the cross sectional area of the flow
path would have to be

$$A = \frac{146}{100 \times 60} = .025 \text{ ft}^2$$

or 0.25 ft high and 0.1 ft wide. For 22 revolutions the cyclone
would have to be at least 22 x .25 or 5.5 ft tall. These figures
clearly indicate that cyclone type devices are not applicable to
the present problem.

Another possible geometric configuration for using centrifugal
forces is one in which the gas flows radially against the
centrifugal force. If we assume a cylinder of 0.5 ft in radius,
then the centrifugal force at 6000 rpm would be

$$F_c = \frac{\omega^2 R_g}{g_c} = \frac{(100 \times 2\pi)^2}{32.2} \times g \times 0.5 = 6100 \text{ gravities}$$

The maximum face velocity which would prevent passage of 1 micron particles would be

$$V_{max} = 6100 \times \frac{7 \times 10^{-3}}{30.5} = 1.4 \text{ ft/sec}$$

For a flow of 146 cfm the length required would be

$$L = \frac{146}{60 \times \quad \times 1.4} = .55 \text{ ft}$$

This size is feasible, that is a cylinder 1 ft in diameter and 0.55 ft long could be accomodated in most motor vehicles. However, operation at 6000 rpm for long periods of time would require expensive construction to assure maintenance free operation. Also, the device would be prohibitively large if it were designed to be efficient on 0.1 micron particles which are known to be present in high concentration in engine exhausts.

Small particles can also be collected by impingement. The efficiency of impingement increases when the size of the target decreases. This principle has been effectively developed for certain applications (Ref. 10).

Consider a wire filament in a plane perpendicular to an airstream containing aerosol droplets of various sizes. The airstream will flow past the filament as shown diagrammatically in Figure 1.

Particles of low inertia may be carried along the flow lines and never reach the filament, but at a critical size the particle inertia will be large enough for it to cross the flow lines and impact on the filament.

It will be seen that d', the effective filament diameter, is defined by the flow pattern for capture of particles not crossing the flow lines. Thus d', shown in Figure 1, is the effective fiber diameter for particles smaller than or the same size as particles just notcrossing flow lines; d' increases with particles size until it reaches a maximum of $(d_f + d_p)$ where d_f is filament diameter and d_p is particle diameter, as shown in Figure 2.
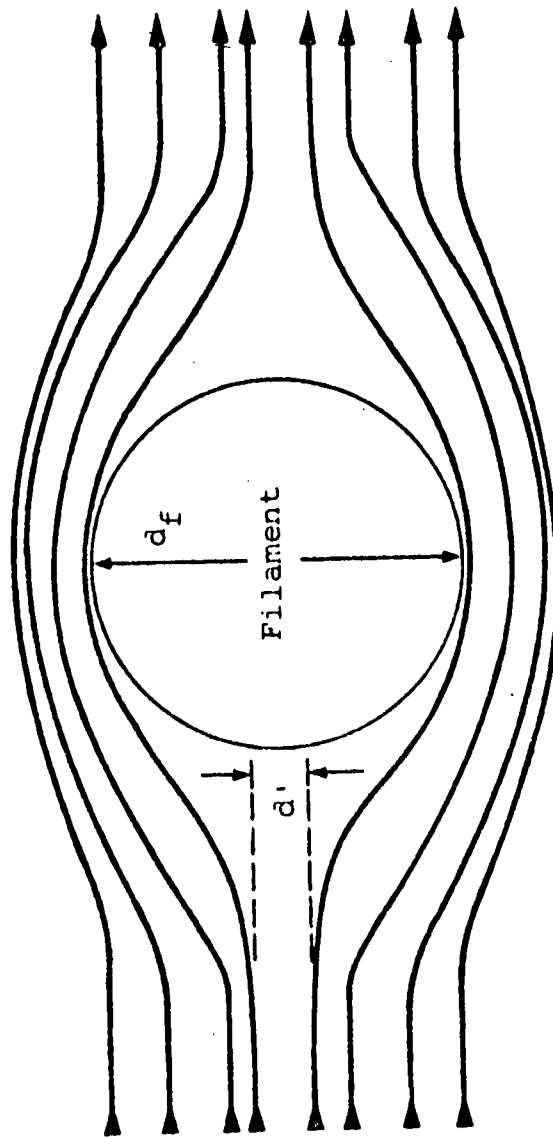
Figure 1

SIMPLIFIED AIRFLOW PAST A FILAMENT
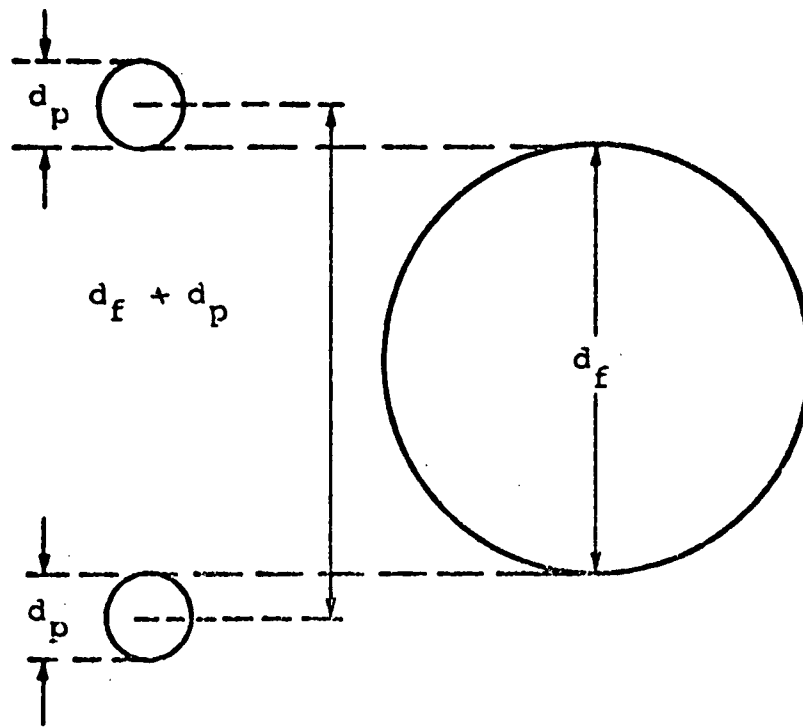
Figure 2

COLLECTION DIAMETER OF A FILAMENT

The ratio d'/d_f is defined as the efficiency of impaction, E_I. The impaction of aerosol particles by differently shaped objects placed in their paths has been studied by Wong et al (Ref. 11). They experimentally determined that the collection efficiency is a function of the inertia parameter, Ψ, and that for circular cylinders the collection efficiency is 90% when Ψ is about 4.0. The inertia parameter, Ψ, is defined by:

$$\Psi = \frac{C\rho_p V d_p^2}{18 \eta d_c} \qquad (5)$$

where

C   is the Cunningham correction factor

ρ_p is the density of the aerosol particles, gm/cm^3

V   is the velocity of the particles relative to the collector, cm/sec

η is the viscosity of the aerosol carrier gas, poise

d_p is the diameter of the aerosol particle, cm

d_c is the diameter of the collecting cylinder, cm

The experimental results of Wong et al agree well with theoretical values of Equation 5, calculated by other workers.

However, even this technique is difficult to apply to low mass submicron sized particles. If a filament diameter of 0.01 cm is assumed to be the smallest practical diameter, it is calculated that a rotational speed of at least 10,000 rpm is required on a brush of at least 18.5 cm radius. These conditions are judged to be too severe for maintenance free operation for long periods of time.

Particles in the submicron size range can be effectively separated by filtration and by electrostatic precipitation. However, the fine filters required for submicron sized particles plug easily and have a relatively high resistance to flow even when clean. Filters for this application would require periodic changing and would be expensive.

Electrostatic precipitators although possessing the

capability of removing submicron particles can do so at the cost of high space and initial cost requirements. Electrostatic precipitators for collecting fly ash operate with retention times of from 1 to 5 seconds (Ref. 12). Thus, to clean 146 scfm of gas would require a minimum precipitator volume of 2.45 cubic feet and this only if the gas were cooled to ambient conditions. The necessary power conditioning equipment can be expected to be expensive and periodic maintenance would be required since efficiency would decrease if electrically resistive deposits accumulated in the precipitator. For these reasons, the electrostatic precipitator is not considered the best approach to the present problem.

This research effort was undertaken to establish the feasibility of developing two high efficiency collection devices for the removal of particulate matter from internal combustion engine exhausts. The first approach is thermal precipitation which makes use of the phenomenon of particle migration and deposition in a temperature gradient. The second technique is based on sonic agglomeration in a fluidized bed.

II. EXPERIMENTAL PROCEDURES

Since it was not feasible to use automobile exhausts directly in the present study, aerosols were generated having a particle size range, concentrations, and other characteristics approximating the lead based constituents found in automobile exhausts.

A.   Aerosol Generation

1. Generation of Carbonaceous Aerosols

Initially, carbonaceous aerosols were generated by incomplete combustion of benzene in a natural gas flame to test the thermal packed bed device. Benzene was allowed to flow through a capillary orifice by gravity feed and drip on the gas flame. The resulting aerosol, consisting of submicron particles, was directed into the packed bed as shown in Figure 3. The generation of carbonaceous aerosols was stopped after preliminary tests, and subsequent experiments were performed with lead chloride aerosols, as suggested by the project officer to obtain data more representative of motor vehicle exhaust.

2. Generation of Lead Chloride Aerosols

The experimental procedure for generating submicron aerosols by vaporization-condensation of lead chloride was similar to that described by Espenscheid et al, for producing sodium chloride (Ref. 13) and silver chloride aerosols (Ref. 14). The technique essentially consists of the passage of a carrier gas through a furnace containing the metal halide. The carrier gas picks up vapor of the material from which aerosol is to be formed in the furnace. The gas-vapor mixture cools after leaving the furnace and condensation of the vapor takes place to form aerosol particles.

A schematic diagram of the experimental setup for producing $PbCl_2$ aerosols by vaporization-condensation technique is shown in Figure 4. A stream of dry filtered air at a flow rate of 20
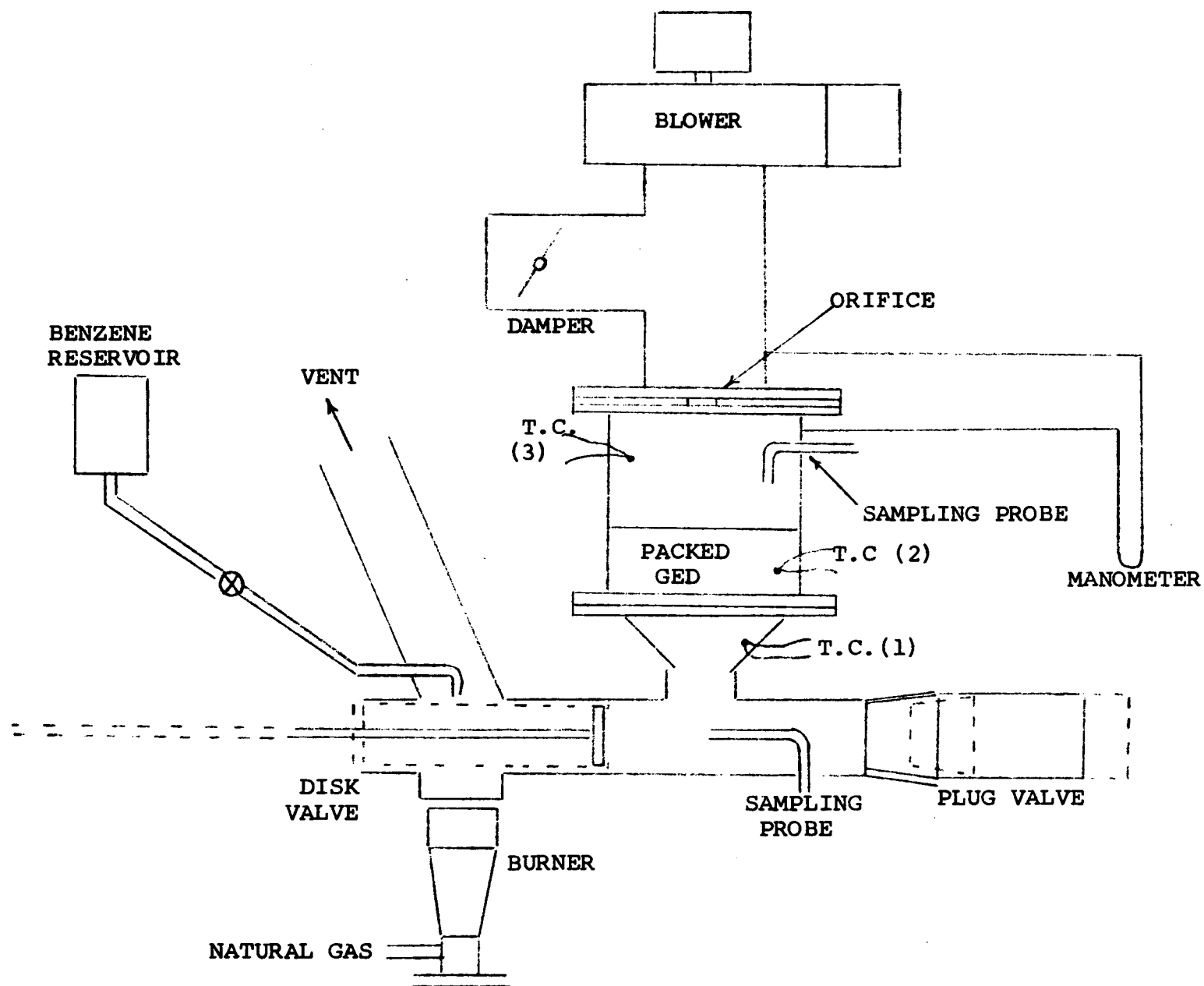
Figure 3 - Schematic Diagram for Generation and Deposition of Carbon Particles in a Packed Bed
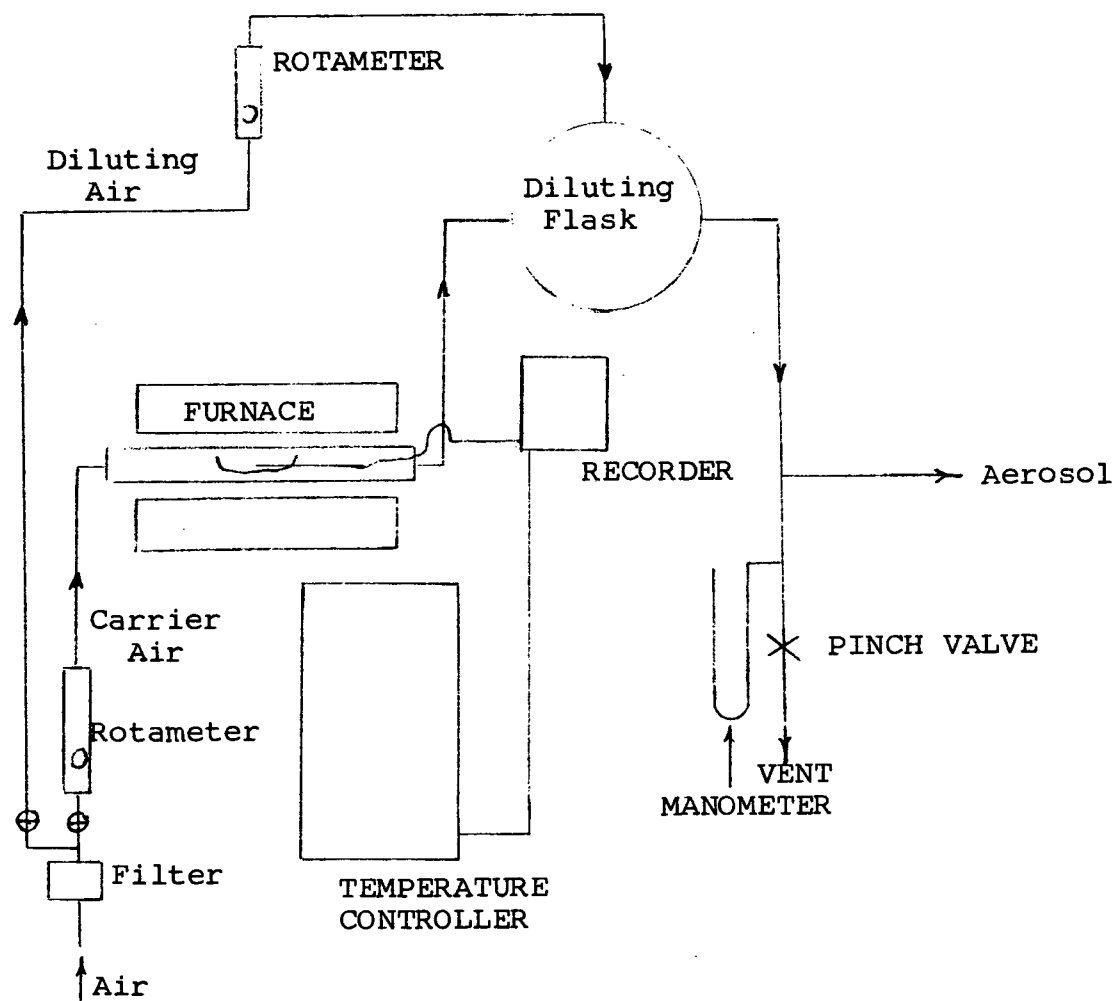
Figure 4 – Schematic Diagram of Lead Chloride Aerosol Generator

liters/minute was directed through a Vycor combustion tube placed in a high temperature furnace. The temperature of the boat containing $PbCl_2$ was monitored by a chromel-alumel thermocouple connected to the inside of the boat. The thermocouple output was fed into a Wheelco model A4897 proportional temperature controller* and a Mosley model 680 recorder**. A stainless steel jacket surrounding the Vycor tube promoted uniform temperature distribution and avoided rapid temperature changes in the boat. The temperature of the melt in the boat was maintained within $\pm$ 10°C of the desired value.

The gas-vapor mixture cooled on leaving the furnace forming lead chloride aerosol by self nucleation. Aerosol coming out of the generator was very concentrated and was diluted with a stream of dry filtered air in a large mixing chamber. The diameter and concentration of lead chloride particles was easily controlled by adjusting the furnace temperature and the flow of diluting air. This technique for generating $PbCl_2$ aerosols showed excellent reproducibility.

The aerosol from the dilution chamber was sampled with an electrostatic precipitator. The particles were deposited on electron-microscope grids coated with a thin film of carbon. The grids were examined with a Hitachi (Model HS-6) electron microscope and photomicrographs of the deposited particles were taken.

The temperature of the furnace was varied at a constant carrier gas flow rate of 20 liters/minute to study the effect of furnace temperature on the particle size distribution of the resulting aerosols. Typical electron photomicrographs of lead chloride particles are shown in Figure 5. Size distributions of the particles were determined from the electron photomicrographs.

---

*Manufactured by Wheelco Instruments, Div. of Barber Colman Co., Rockford, Illinois.

**Manufactured by Mosley Div., Hewlett Packard, Pasadena, California.
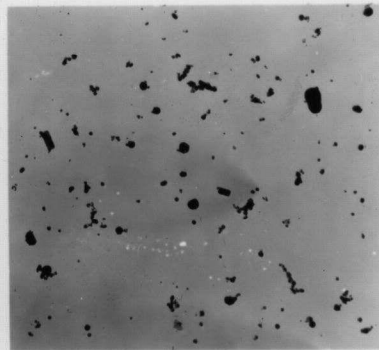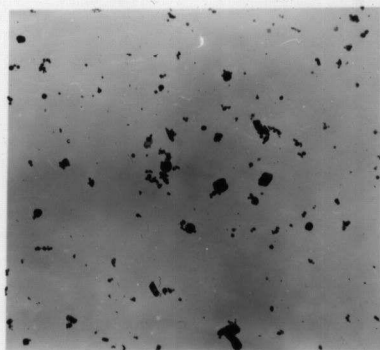
Furnace: 390°C
Carrier Flow: 20 l/min
MMD.   0.216μ
10,000 Magnification
1 cm = 1μ
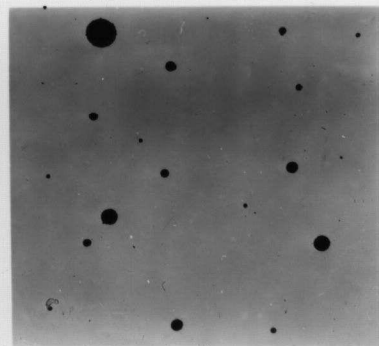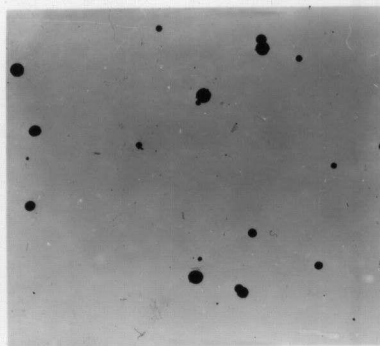
Furnace: 450°C
Carrier Flow: 20 l/min
MMD.   0.487μ
5,000 Magnification
1 cm = 2.0μ

Figure 5:   Photomicrograph of Lead Chloride Particles
at Different Furnace Temperatures.

Table II shows a typical particle size distribution obtained during the calibration of the aerosol generator. Figure 6 shows the size distribution of aerosol particles at four furnace temperatures on log probability paper.

The effect of furnace temperature on frequency mean diameter and mass mean diameter has been plotted on Figures 7 and 8 respectively. Figure 8 was used to generate aerosols of known mass mean diameters during subsequent experiments with the packed bed and the fluidized bed.

B.   Analytical Techniques

The concentration of carbonaceous aerosols was determined using a reflectometer. The concentration of $PbCl_2$ aerosols was determined using polarographic and colorimetric techniques. The experimental procedures and calibration curves are given in Appendix I.

Table II

A TYPICAL PARTICLE SIZE DISTRIBUTION OF LEAD AEROSOLS

Furnace Temp.   = 468°C
Carrier Gas Flow = 20 lit/min
Dilution Flow   = 16 lit/min

Size, μ	Number Count	Cumulative Count	% Equal to or Greater Than Indicated Size
0.025-0.049	30	30	76
0.049-0.098	58	88	29.6
0.098-0.196	26	114	8.8
0.196-0.295	9	123	1.6
0.295-0.394	1	124	0.8
	n+1	125	
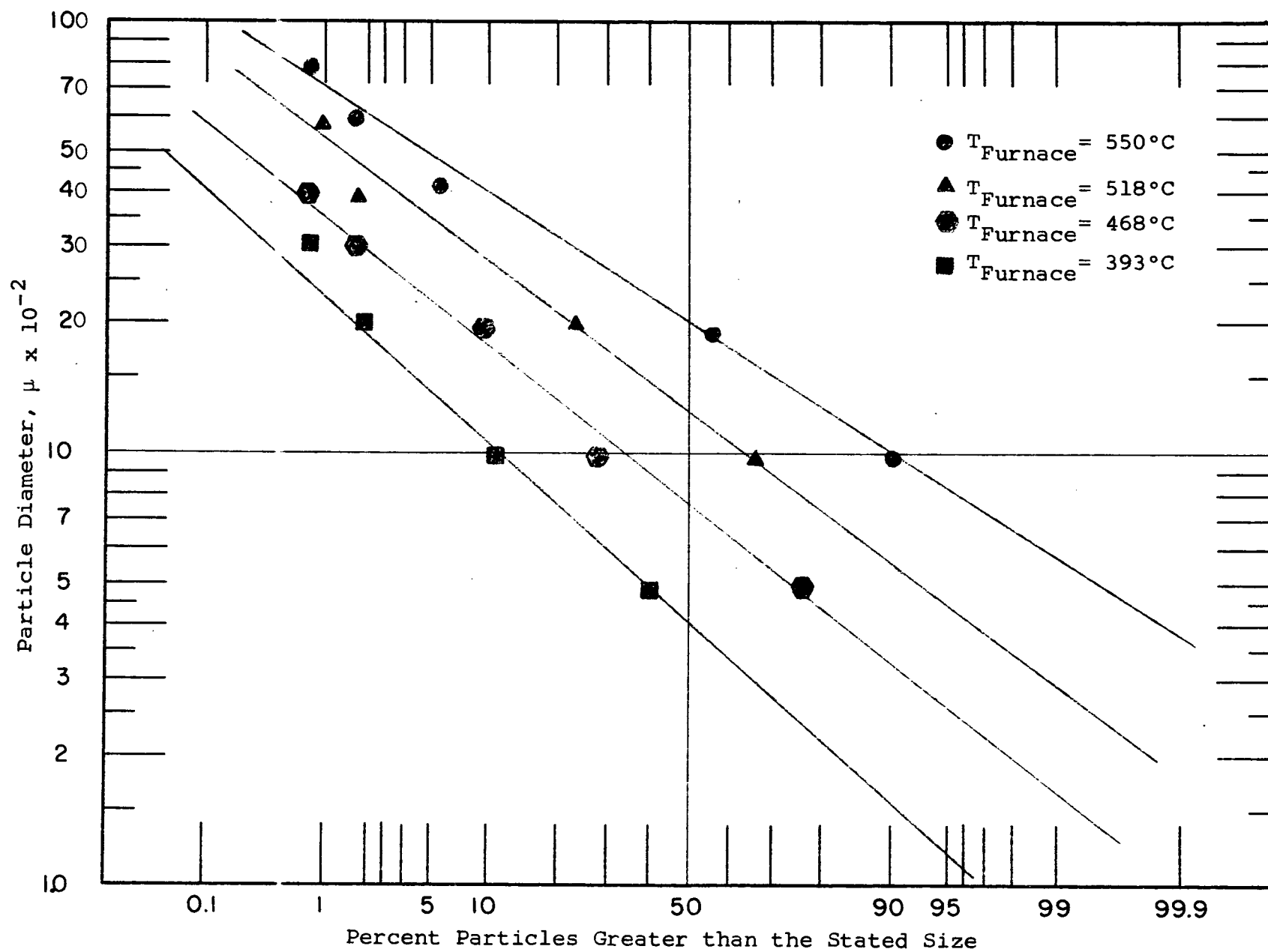
Figure 6 – Particle Size Distributions of Lead Chloride Aerosols at Different Furnace Temperatures
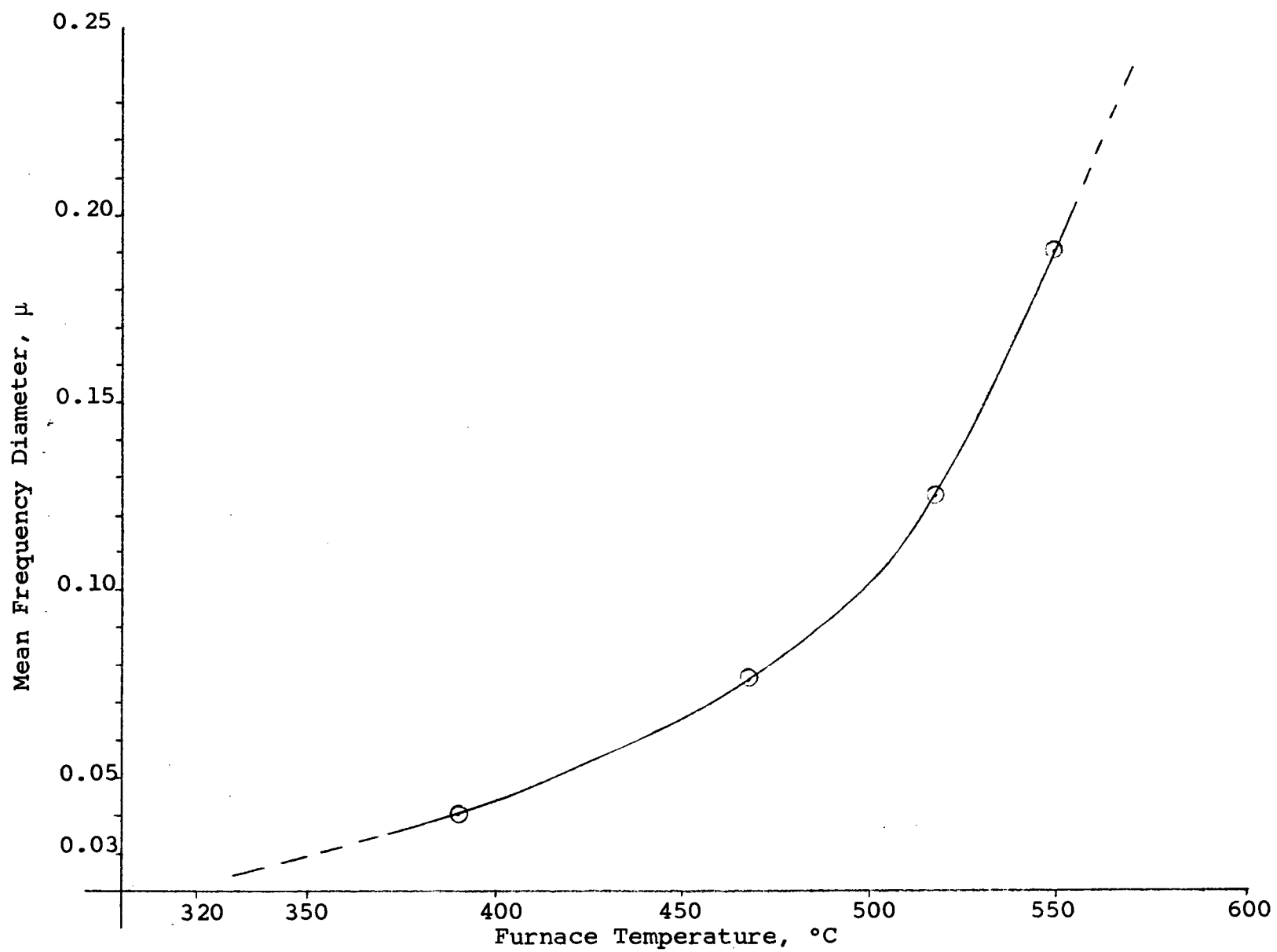
Figure 7 – Effect of Furnace Temperature on Mean Frequency Diameter of Aerosol Particles

18
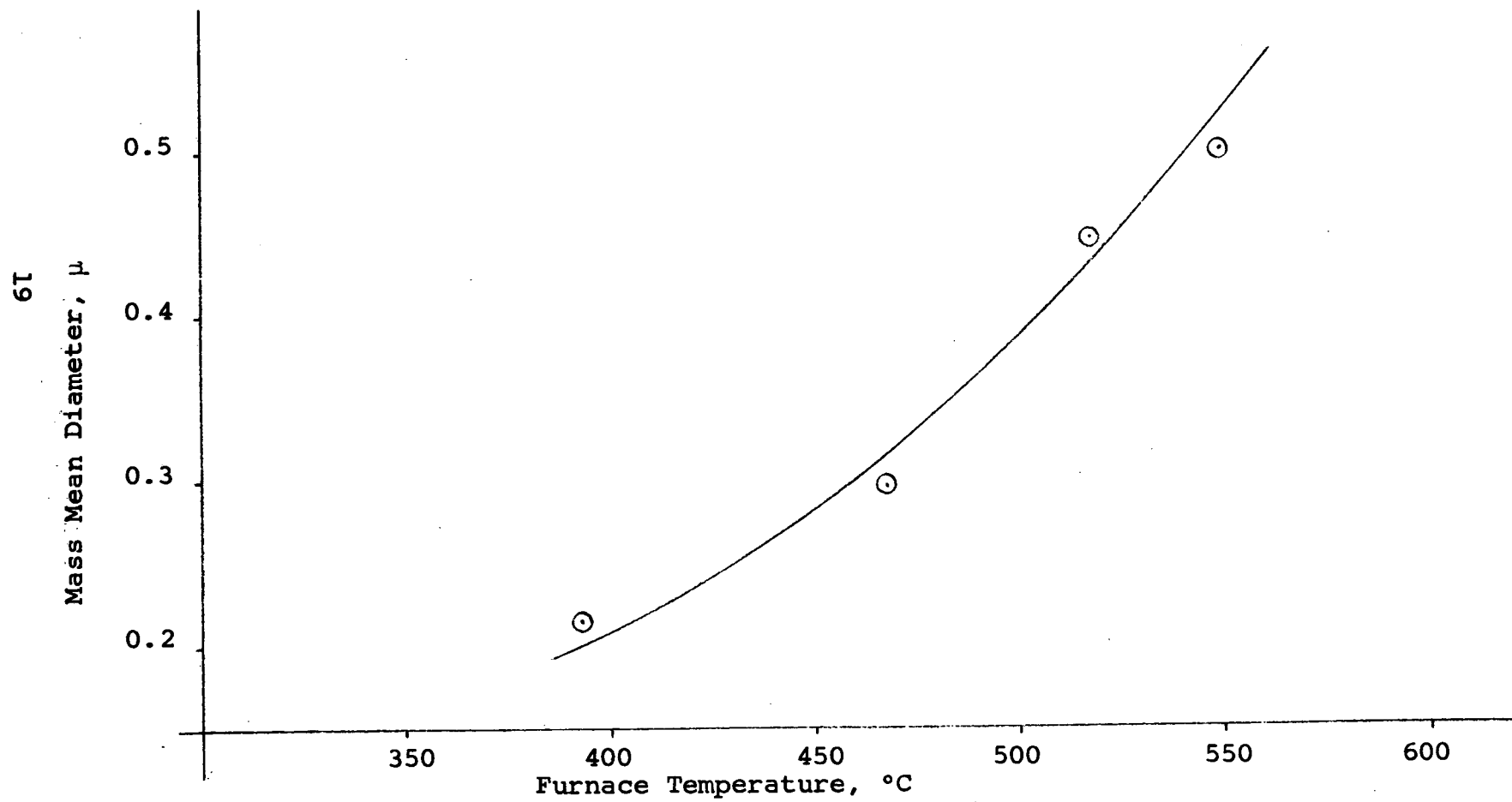
Figure 8 - Effect of Furnace Temperature on Mass Mean Diameter of Aerosol Particles

III. THERMAL PACKED BED DEVICE

The motion of small particles suspended in a gas stream under the influence of thermal gradients has been the subject of many investigations (Ref. 15,16,17). Particles move from hot gas streams to cold surfaces under the influence of thermal forces. A particle in a thermal gradient can be expected to be hotter on one side than on the other. Gas molecules striking the hot side, on the average, will rebound at a higher temperature and hence, a higher velocity than those striking the cold side. This imbalance creates a force on the particle directed toward the colder end of the temperature gradient. This phenomenon is well known and is used in commercially available thermal precipitators used to collect submicron sized aerosols with virtually 100 percent efficiency. A more familiar example of the same phenomenon is the cold wall in a room which always gets dirtier sooner than the warmer walls.

Although the thermal precipitation effect is well known and apparently has been shown to be effective to some degree for the present application, the principle has not yet been applied to an optimum degree. Best results can be expected when thermal gradients are maximized and migration distance minimized. A packed bed of high heat capacity material appears to have these desired properties.

A. Description of Experimental Setup for Thermal Deposition Studies

The laboratory experimental setup of the apparatus for thermal deposition studies in a packed bed is shown in Figure 9. The packed bed device, 28 cm high and 12.1 cm diameter, was constructed from 11 gauge, 304 stainless steel to eliminate corrosion of the inside walls. A coarse retaining screen was welded to the bottom of the shell. The cylindrical shell was packed with the desired packing material by pouring the material from the top and tapping the sides of the bed to obtain uniform
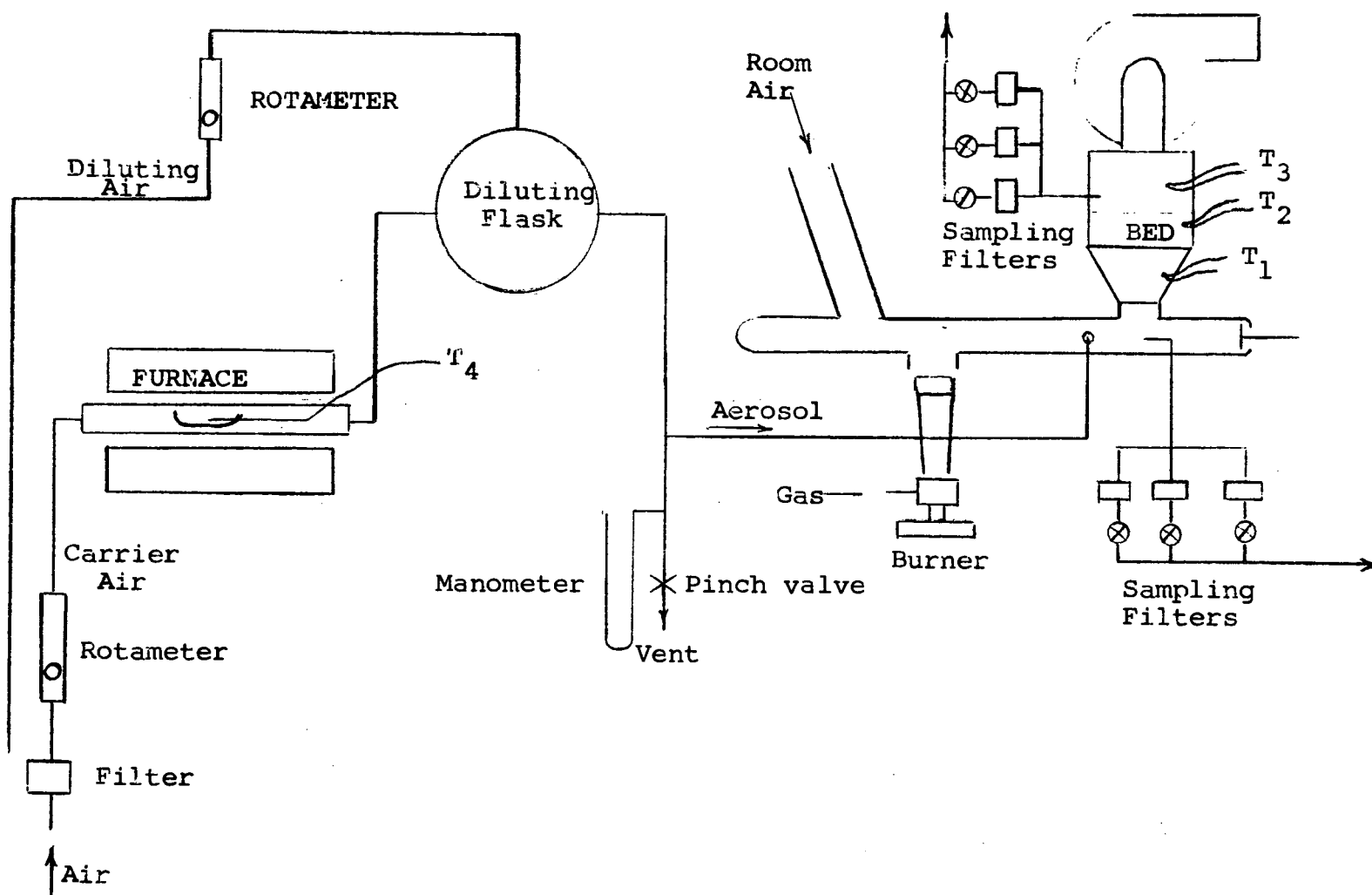
Figure 9: Apparatus for Study of Thermal Deposition of Lead
Chloride Aerosol in a Cold Packed Bed

packing density within the bed. The packing height was kept constant for all tests and the weight of different packing materials to fill the bed to a depth of 7.6 cm above the retaining screen was determined. The bed was insulated on the outside with a 1.5 cm layer of pipe insulation to prevent particle deposition on the walls and to minimize the heat losses.

The unit was designed to allow simultaneous determinations of the upstream gas temperature (T_1), apparent bed temperature (T_2), and the effluent gas temperature (T_3). The temperature profiles T_1 and T_2 with time were monitored simultaneously with a Bristol multipoint recorder*. The downstream effluent temperature (T_3) was recorded using a Mosley 620 recorder**.

A small portion of the aerosol stream leaving the dilution flask was fed into the simulated exhaust pipe where it was mixed with room air. The blower on top of the packed bed was turned on along with a burner which heated the room air stream. The flow rate of air containing $PbCl_2$ particles through the bed was controlled by adjusting a damper downstream of the bed. The flow rate was determined by monitoring the pressure drop across a 2.5 cm diameter calibrated orifice. This way the superficial velocity through the bed could be varied from 15 cm/sec to 130 cm/sec. The pressure drop across the packing was also recorded.

B. Determination of the Collection Efficiency of the Thermal Packed Bed Device

The collection efficiency of the packed bed device was determined by simultaneous sampling of the gas stream both upstream and downstream of the bed. Identical sampling lines were constructed from 6 mm stainless steel tubing and connected to sampling probes inserted both upstream and downstream of the

*Manufactured by the Bristol Co., Waterbury, Connecticut

**Manufactured by Hewlett Packard, Pasadena, California

packed bed. The sampling probes could be moved in the radial direction to get a complete concentration traverse. Initial tests showed that aerosol concentration did not change with radial position of the probe. All subsequent sampling was performed by positioning the probes at the axis of the bed. However, the sampling was not isokinetic. Since isokinetic sampling is unimportant for submicron particles, anisokinetic sampling did not introduce any significant error in concentration measurements. The other ends of the sampling lines were connected to sampling banks and all exposed portions of the lines were kept at 300°C with electrical heating tapes to prevent particle loss due to thermal deposition on the inside walls of the sampling lines. Each sampling bank contained three Millipore filter holders with 2.5 cm diameter Gelman Type A fiber glass filters. The filter holders were connected to solenoid valves to permit simultaneous sampling of aerosol streams on both ends of the bed. The sampling banks were connected to a vacuum pump through calibrated flow restriction orifices. This sampling procedure allowed three sets of samples to be taken during a test run. The downstream orifice was selected to sample at a higher flow rate than the upstream orifice because of low concentrations to be expected at the downstream of the bed. A typical test run with the packed bed proceeded as follows:

The aerosol generator furnace temperature was preset on the temperature control unit to give the desired aerosol size using Figure 8. The carrier and dilution air flow rates were adjusted to 20 and 16 lpm respectively.

At steady furnace temperature, the aerosol stream from the dilution chamber was connected to the bed and mixed with heated room air in the simulated exhaust pipe. The damper was adjusted to give the desired gas velocity through the bed and the temperature recorders for monitoring T_1, T_2 and T_3 were engaged. The upstream gas temperature, T_1, was brought to the desired value by adjusting the gas burner. The bed temperature, T_2, at

the onset of the test run was low and the gas-packing temperature differential (T_1-T_2) was large. The bed heated up with time on the passage of hot air containing lead chloride particles, thus reducing the gas-packing temperature difference.

Aerosol samples were collected both upstream and downstream of the bed for one minute by activating a set of solenoid valves. Temperatures T_1, T_2 and T_3 were marked on the charts. The same procedure was repeated at two higher bed temperatures to obtain three sets of samples during a test run. At the completion of a test run, the aerosol stream was disconnected, the burner was shut off, and the bed allowed to cool.

Three sets of samples obtained at different ΔT values were then analyzed for lead using either the polarographic or the colorimetric technique (see Appendix I). The concentration of $PbCl_2$ in the gas stream was calculated from the analytical results and the volume of aerosol sampled. The collection efficiency, E, of the thermal packed bed device was calculated from:

$$E = \frac{C_o - C_1}{C_o} \times 100\% \qquad (6)$$

where,

C_o = upstream aerosol concentration, μg $PbCl_2$/liter

C_1 = downstream aerosol concentration, μg $PbCl_2$/liter

C. Experimental Data and Discussion of Results

Initially tests were conducted using carbonaceous aerosols and a bed packed with 8 mm glass helices to a depth of 5.7 cm. Filter samples were collected on both the upstream and the downstream of the bed at a gas-packing temperature difference of 600°C.

The reflectivity of the filters shown in Figure 10 was measured with a reflectometer. The collection efficiency was calculated from the reflectance measurements using Equation 4-A (See Appendix I). The collection efficiency of the thermal
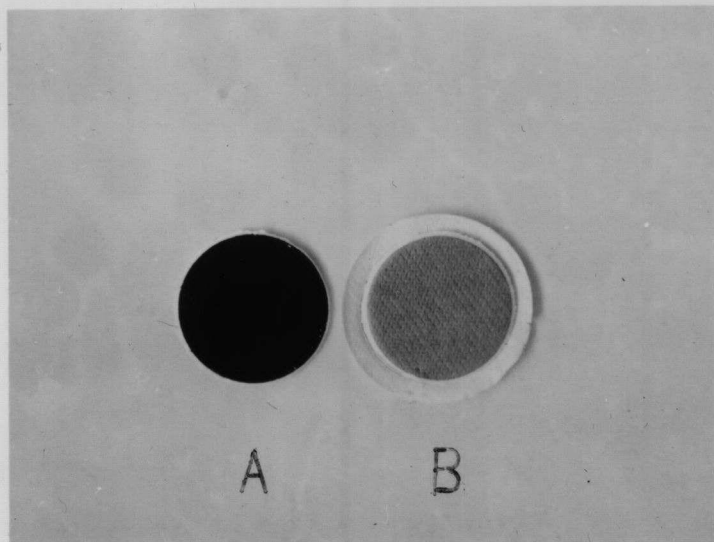
Test 1 – A – Upstream sample, 2% Reflectivity
        B – Downstream sample, 31% Reflectivity
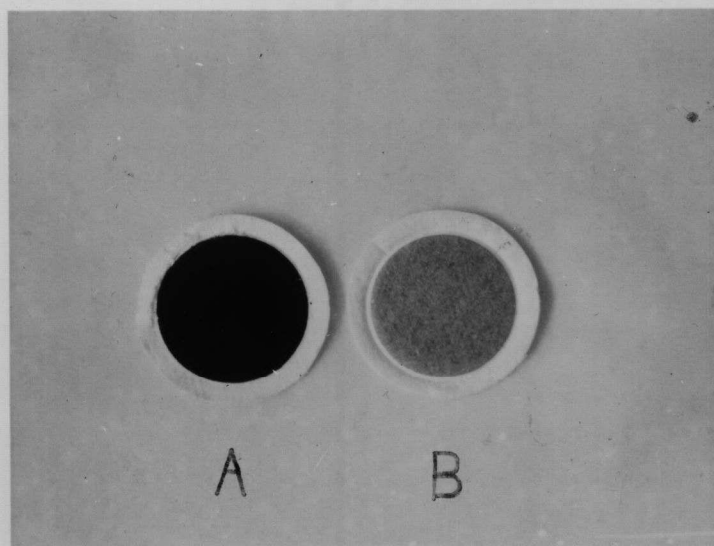
Test 2 – A – Upstream sample, 2% Reflectivity
        B – Downstream sample, 31% Reflectivity

Figure 10 – Filters from Thermal System Tests

packed bed device for carbonaceous particles was found to be
68%. This value of collection efficiency is not very accurate
since the Beer-Lambert Law does not apply to very dark surfaces.
Subsequent experimental work was done using $PbCl_2$ aerosols as
the test material.

A series of experimental tests were performed with the
thermal packed bed to study the effect of particle size, size and
shape of the packing, heat capacity of the packing material, gas
velocity through the bed, concentration of the aerosol,
contamination buildup on the packing material, and the gas-packing
temperature difference on the collection efficiency of the bed.
All experimental data obtained using $PbCl_2$ particles as test
aerosols are presented in Table III.

During the course of an experiment ΔT changes not only with
time but also with position within the bed because the upstream
side of the packing is heated at a faster rate than the downstream
side. Moreover, a thermocouple inserted into the bed does not
accurately measure the packing surface temperature. Although
the relationship between thermocouple reading to the bed surface
temperature is not known, the thermocouple reading can be used as
a parameter since a definite relationship between the two values
must exist. The gas-packing temperature difference is a measure
of the thermal force acting between the aerosol particles and the
packing surface. Therefore, all collection efficiency data have
been correlated with the apparent gas-packing temperature
difference ΔT, (T_1-T_2).

In Table III, the temperatures T_1, T_2 and T_3 refer to the
upstream, bed and downstream temperatures, respectively. Since
obtaining a sufficiently large aerosol sample for analysis
required sampling for periods from several seconds to one minute,
these temperatures changed slightly during the sampling period.
Therefore, the values indicated in Table III represent time average
values of the temperatures during the sampling period.

The velocity through the bed, V_B, has been calculated as a

Table III

COLLECTION EFFICIENCY DATA ON THE THERMAL PACKED BED DEVICE

Test No.	T_1, °C	T_2, °C	T_3, °C	ΔT_{1-2}, °C	MM D, μ	V_B, cm/sec	ΔP_{bed}, cm H_2O	C_o, μg/liter	% EFF	Packing
2-14-70	27	27	27	0	0.45	15.5	0.73	29.4	41	Helices
2-14	27	27	27	0	0.45	15.5	0.73	16.0	37	Helices
2-14	27	27	27	0	0.45	15.5	0.73	14.6	34	Helices
2-19	220	96	34	124	0.48	26.2	0.73	29.3	87	Helices
	234	156	42	78	0.48	27.4	0.73	61.0	66	Helices
	266	208	67	58	0.48	27.0	0.73	17.1	69	Helices
2-20	234	170	30	167	0.30	20.7	1.04	2.4	>95	Helices
	226	138	42	88	0.30	20.7	1.02	2.2	71	Helices
	226	178	61	48	0.30	24.9	.97	2.7	66	Helices
2-27	227	103	45	125	0.30	20.6	.97	3.2	66	Helices
	227	170	73	58	0.30	22.4	.97	2.4	57	Helices
	222	211	103	58	0.30	16.1	.97	2.4	5	Helices
3-2	191	55	32	147	0.35	25.7	1.2	1.2	95	Helices
	218	134	59	84	0.35	27.7	1.5	1.2	90	Helices
	226	205	128	20	0.35	26.4	1.3	1.2	12	Helices
3-3	231	107	39	124	0.54	28.8	1.5	12.2	66	Helices
	222	182	63	40	0.54	27.4	1.5	17.1	50	Helices
	238	218	113	20	0.54	25.6	1.5	14.6	42	Helices
3-6	237	80	33	57	0.47	23.4	1.8	7.3	87	Helices
	266	167	50	99	0.50	24.5	1.8	14.6	54	Helices
	274	228	88	46	0.50	27.0	1.8	14.6	53	Helices
3-10	231	70	34	161	0.36	25.4	2.5	1.2	>95	Helices
	225	150	43	75	0.36	25.4	2.5	1.6	85	Helices
	230	215	77	153	0.36	22.3	2.5	1.2	68	Helices
3-30	226	33	30	193	0.33	15.5	0.71	1.2	95	6mm Glass Spheres
	226	41	30	185	0.33	15.5	0.71	1.6	85	
	218	50	30	168	0.33	15.5	0.71	1.2	69	
4-14	207	41	30	166	0.45	15.5	0.71	14.6	66	
	223	131	66	92	0.45	15.5	0.71	9.8	67	
	218	200	126	18	0.45	15.5	0.71	29.	33	
7-15	211	25	27	186	0.45	15.5	0.63	24.4	38	
	222	100	57	122	0.45	15.5	0.63	24.	40	
	215	160	83	55	0.45	15.5	0.68	26.	30	
6-23-70/1	27	27	27	0	0.35	15.5	0.56	35	27	6mm Ceramic Spheres
6-23-70/2	218	40	30	178	0.35	15.5	0.56	51	95	
	222	142	42	80	0.35	15.5	0.56	39	34	
	211	195	105	16	0.35	15.5	0.56	41.5	24	
6-25-70/1	225	80	30	145	0.35	15.5	0.56	74	77	
6-25-70/3	231	46	26	185	0.35	15.5	0.56	9	>95	
	222	101	31	121	0.35	15.5	0.56	25	56	
8-4	25	25	25	0	0.28	15.5	0.56	1	26	
8-5-70/1	237	33	33	234	0.28	15.5	0.56	1	>95	
	218	109	99	109	0.28	15.5	0.56	1	50	
	226	146	156	80	0.28	15.5	0.56	1	30	
8-5-70/2	218	59	35	159	0.28	15.5	0.56	1	72	
	222	128	61	94	0.28	15.5	0.56	1	46	
	222	170	101	52	0.28	15.5	0.56	1	27	
8-6-70/1	236	36	35	200	0.35	15.5	0.56	21	97	6mm Steel Spheres
	226	41	35	185	0.35	15.5	0.56	24	84	
	231	76	35	155	0.35	15.5	0.56	27	83	
8-6-70/2	227	99	56	128	0.35	15.5	0.56	22	75	
	227	151	81	76	0.35	15.5	0.56	23	36	
	227	185	108	42	0.35	15.5	0.56	10	30	
8-13-70/1	25	25	25	0	0.35	15.5	0.56	156	27	
8-13-70/2	226	135	25	91	0.35	15.5	0.56	91	34	
	218	165	25	53	0.35	15.5	0.56	100	24	
8-13-70/3	223	34	25	189	0.35	15.5	0.56	130	84	
	218	55	25	163	0.35	15.5	0.56	96	--	
	215	101	25	114	0.35	15.5	0.56	118	44	
8-17	218	57	39	161	0.35	89	6	5	73	
	229	143	74	86	0.35	89	6	7	42	
8-20	215	66	40	149	0.35	89	6	87	81	
	218	154	81	64	0.35	89	6	103	--	
	222	194	124	28	0.35	89	6	56	28	
8-28	222	183	118	39	0.35	89	6	76	35	
9-3-70/1	25	25	25	0	0.43	129	10.2	40.5	34	
9-3-70/2	223	97	56	126	0.43	129	10.2	140	59	
9-8-70/1	221	76	40	145	0.43	129	10.2	74	51	
	243	165	100	78	0.43	129	10.2	59	24	
9-9	211	41	95	170	0.43	129	10.2	46	59	
	264	47	34	217	0.43	129	10.2	22	87	
9-11	198	28	25	170	0.33	15.5	0.5	102	98	Contaminate 6 mm Steel Spheres
	222	63	34	159	0.33	15.5	0.5	102	93	
	215	100	49	115	0.33	15.5	0.5	110	70	
	231	143	75	88	0.33	15.5	0.5	96	37	
	213	174	100	39	0.33	15.5	0.5	150	37	

superficial velocity as if the packing occupied no volume, and
with the assumption that the gas was at temperature T_1.

1. Effect of Particle Size on Collection Efficiency

The deposition of submicron particles under the influence
of a thermal force is believed to be independent of particle
size. This was confirmed during initial tests when aerosol
samples collected on the upstream and downstream of the bed were
examined with an electron microscope. While the concentration
of particles in the downstream samples was much smaller than the
upstream samples, the two size distributions were found to be
nearly identical. This suggests that particles in the size range
0.1-0.8 μ were collected by the packed bed device with nearly
the same efficiency. Further tests were conducted using aerosols
having 0.30-0.55 μ mass mean diameters.

2. Effect of Surface Area and Shape of the Packing on Collection Efficiency

The effect of surface area and shape of the packing on
collection efficiency of the thermal packed bed device was
determined using 8 mm diameter glass helices and 6 mm diameter
glass beads. Experiments were performed by loading the bed with
either packing to a depth of 7.6 cm. The total surface area of
the packings in the bed was calculated to be 2.94 x 10^4 cm^2 and
0.54 x 10^4 cm^2 for the helices and beads respectively. Tests
were conducted at a constant gas velocity of 15.5 cm/sec using
$PbCl_2$ aerosols in the size range 0.30-0.55 μ MMD.

The effect of packing shape and surface area on collection
efficiency is shown in Figures 11 and 12. Figure 11 shows that
the collection efficiency of helices is higher than that of glass
beads. The figure also shows that the collection efficiency of
helices increases more rapidly with increasing ΔT compared to
glass beads. This can be explained as follows:

The helices, which pack more compactly compared to spherical
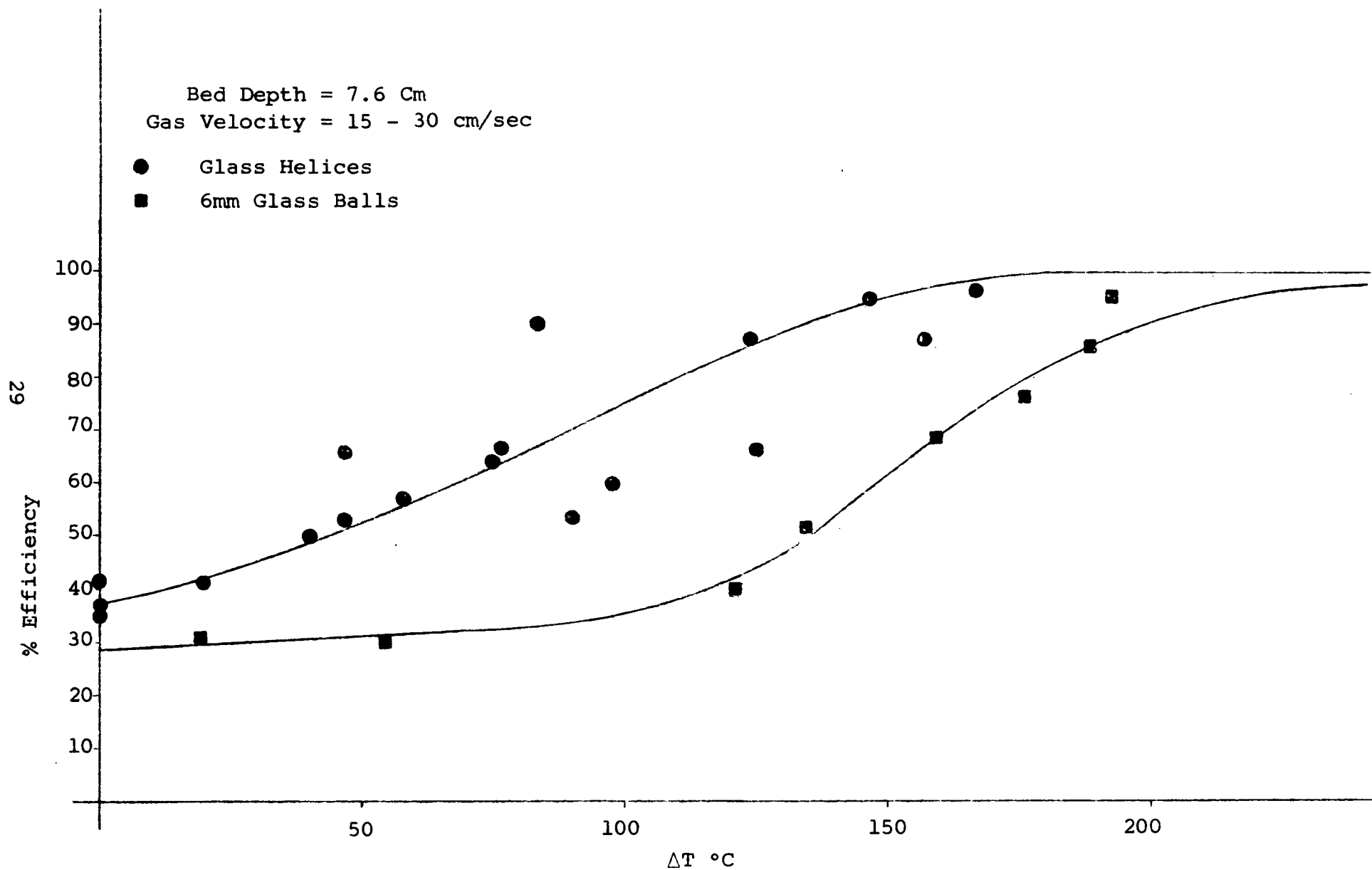
Figure 11 - Effect of the Shape of the Packing On Collection Efficiency of $PbCl_2$ Particles by the Thermal Packed Bed
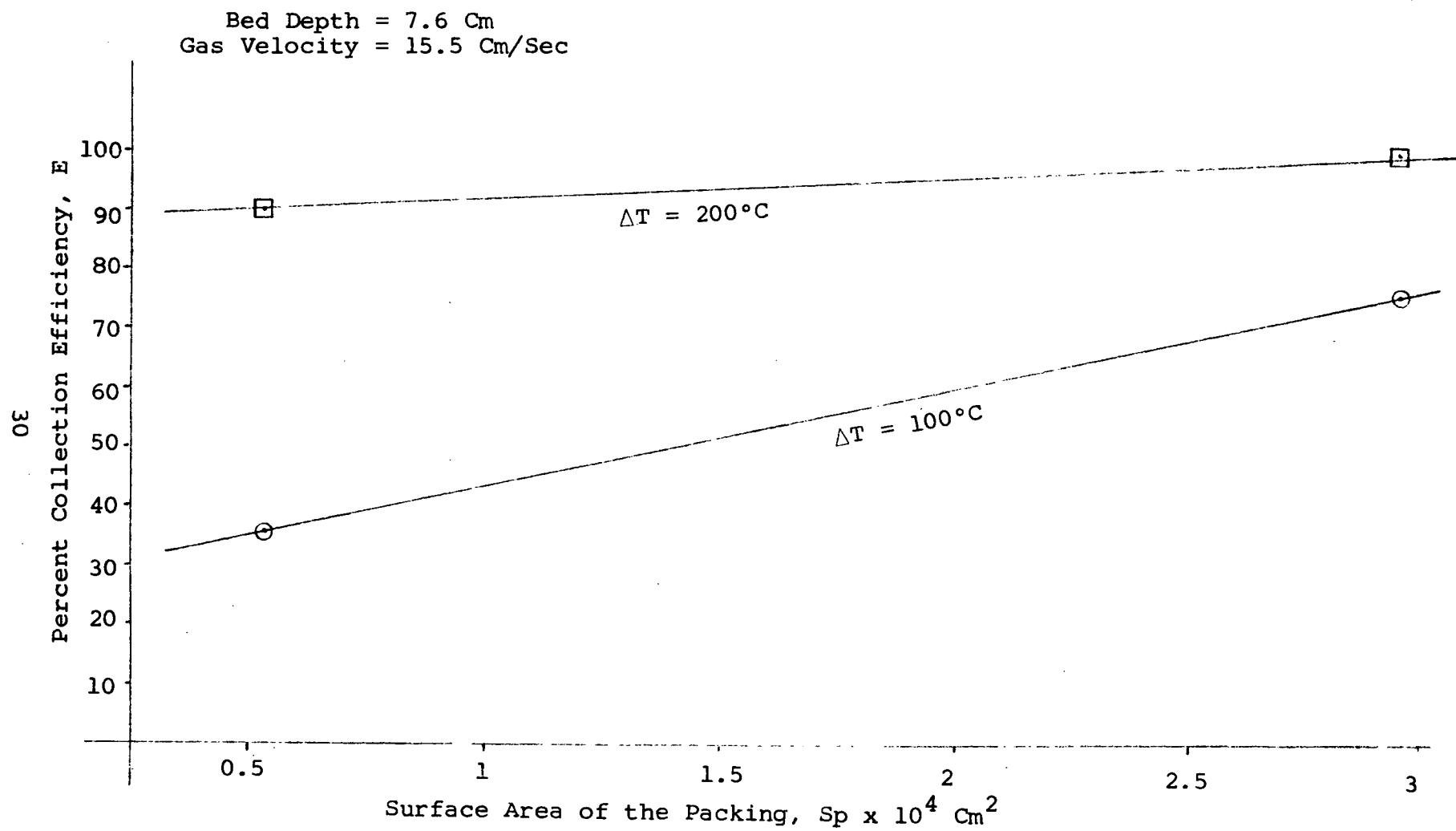
Figure 12 – Effect of Surface Area on Collection Efficiency of $PbCl_2$ Particles by the Thermal Packed Bed

beads, have a higher collection efficiency due to the increased filtration effect in the bed. Moreover, in the case of helices the particle migration distance is very much smaller than that for spheres, causing a higher collection efficiency by thermal deposition. Figure 12 shows the effect of surface area on collection efficiency at different values of ΔT. At low value of ΔT (100°C) the collection efficiency of the bed increases rapidly with increasing surface area compared to that at higher value of ΔT (200°C). It seems that at high gas-packing temperature differences, the temperature gradient at the packing surface becomes the controlling particle deposition mechanism, and surface area of the packing has a relatively small effect.

3. Effect of Heat Capacity of the Packing Material on Collection Efficiency

Effect of heat capacity of the packing on collection efficiency of the thermal packed bed device was determined using 6 mm glass, ceramic, and chrome-steel balls having heat capacities of 0.16, 0.26 and 0.11 gm calories/gm°C respectively. The bed height and gas velocity were kept constant at 7.6 cm and 15.5 cm/sec. Experiments were performed using aerosols in the size range 0.30-0.45 μ MMD at a concentration of approximately 12-25 μg $PbCl_2$/liter. Figure 13 shows that the collection efficiency of the bed is independent of the packing material at small values of ΔT (<80°C). This would be expected since at low gas-packing temperature differences thermal forces are negligible and the particle capture is due to aerodynamic forces only. At constant bed height, gas flow rate and packing shape, the aerodynamic capture of the particles would be independent of the heat capacity of the material. At higher values of ΔT, the collection efficiency of the bed seems to depend on the nature of the packing material. However, there is no systematic change in collection efficiency with heat capacity of the packing material. The bed packed with 6 mm glass beads, which have an intermediate
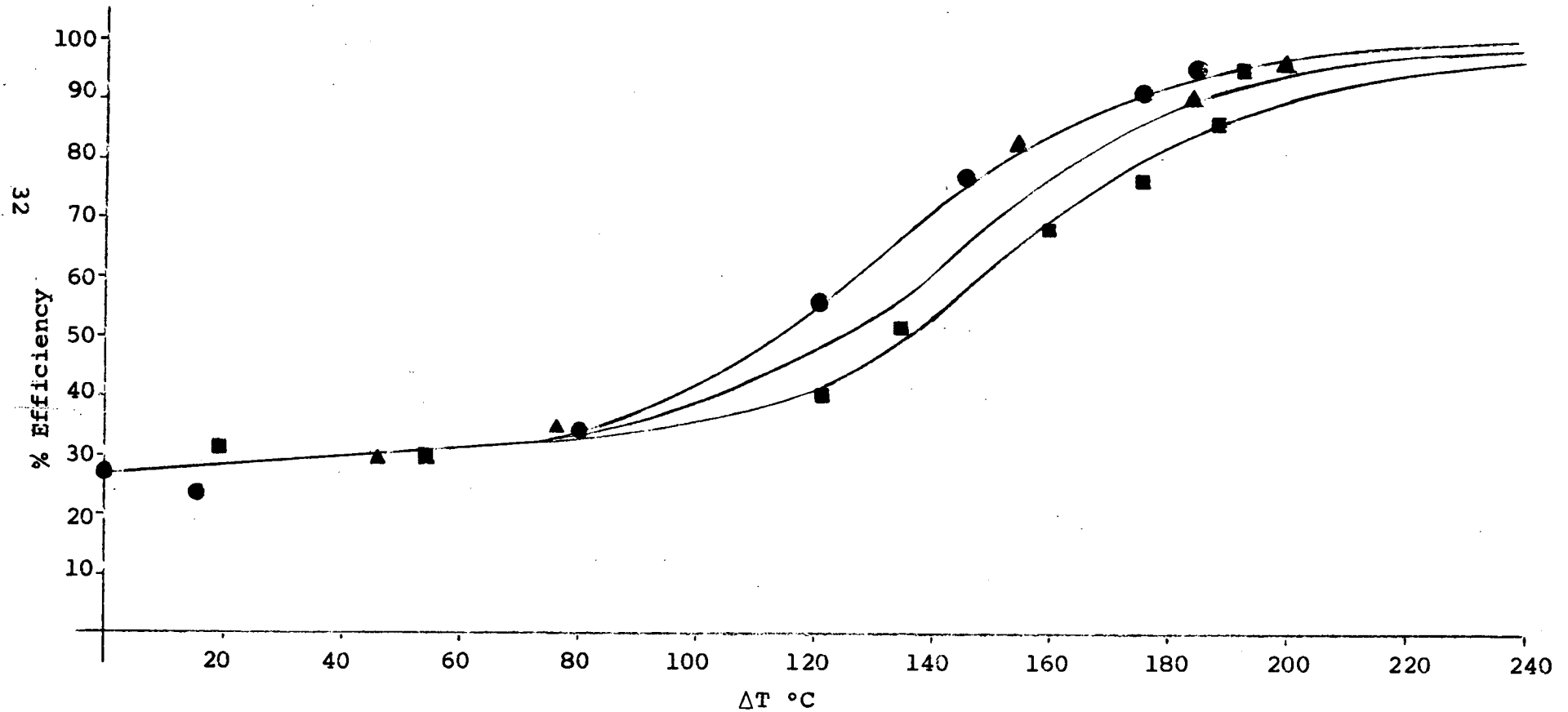
Fig. 13 - Effect of Bed Material on Collection Efficiency of the Thermal Bed

value of heat capacity between steel and ceramic balls, has the lowest collection efficiency for all values of $\Delta T > 80°C$. The higher collection efficiency with ceramic packing is attributed to the rough surface characteristics of the ceramic balls compared to steel and glass balls.

Figure 14 shows the effect of packing material on the heating characteristics of the bed packed to a constant height of 7.6 cm. Even though the packings occupied a constant volume in the bed their mass was different due to variations in density. Therefore, the total heat capacity of the bed varied significantly for the three materials used as shown in Table IV.

Table IV

EFFECT OF PACKING MATERIAL
ON THE TOTAL HEAT CAPACITY OF THE BED

Bed Diameter = 12.1 cm, Bed Height = 7.6 cm
Gas Velocity = 15.5 cm/sec

Packing Material	Mass of Packing In The Bed, gm	Heat Capacity, gm Calories/gm°C	Total Heat Capacity Of The Bed gm Calories/°C
6 mm Glass Spheres	1360	0.16	217.6
6 mm Ceramic Spheres	1176	0.26	305.8
6 mm Steel Spheres	8607	0.11	946.8

From the heating curves shown in Figure 14, it is evident that it is possible to maintain a high gas-packing temperature difference for a longer period of time by using a high heat capacity bed. Figure 15 shows the change in collection efficiency of the packed bed device with time. Initially, when the bed is cold (or gas-packing temperature difference is high), the collection efficiency of the device is high for all packings.

Bed Height   -   7.6 cm
Bed Velocity - 15.5 cm/sec
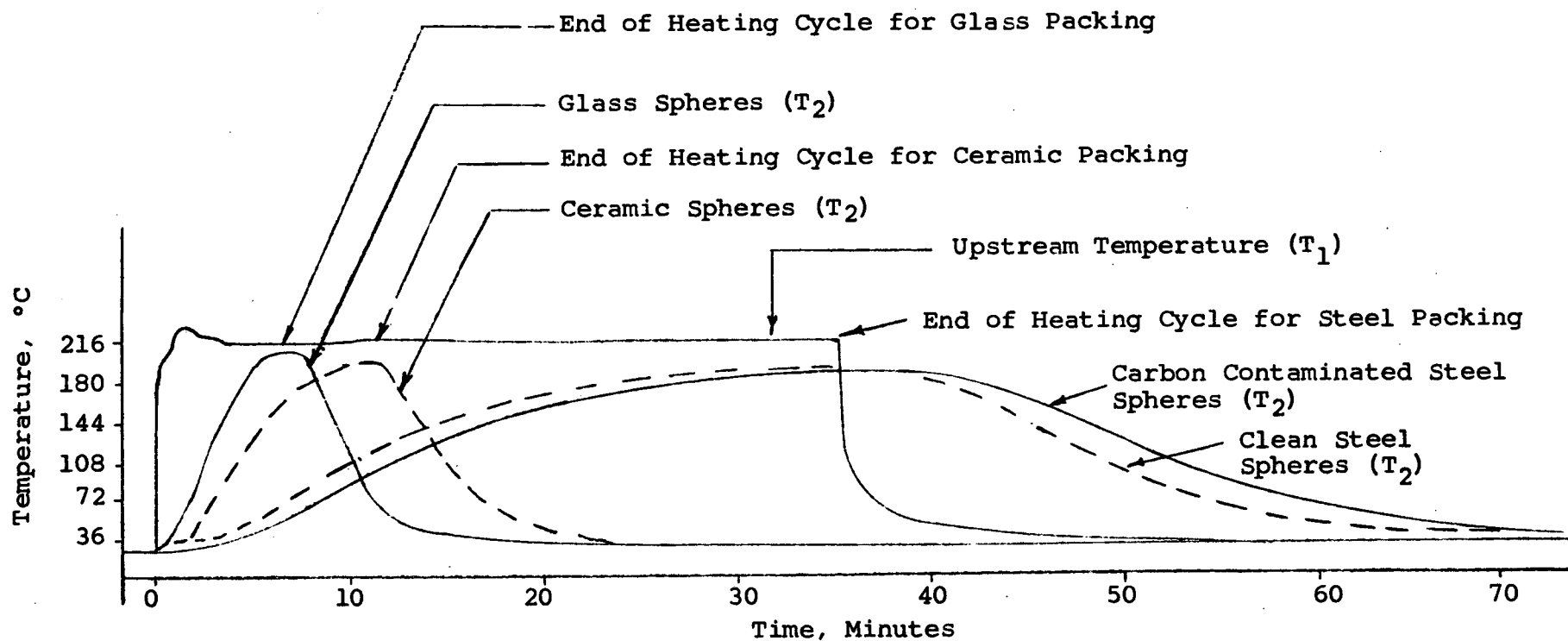
Figure 14:   Effect of Heat Capacity of Packing Material
on Heating Rate of the Packed Bed Device

34

Figure 15: Collection Efficiency of the Thermal Packed Bed Device as a Function of Time

The collection efficiency of beds packed with ceramic or glass spheres, however, decreases rapidly with time compared to the bed packed with steel spheres. Figure 15 also shows that beds packed with steel spheres will operate with efficiencies greater than 90% for four minutes compared to 1.5 minutes for beds containing glass or ceramic packings.

4. Effect of Gas Velocity on Collection Efficiency

The effect of superficial gas velocity on the collection efficiency of the thermal packed bed device was studied using 6 mm steel balls as the packing material. Figure 16 shows that there is no apparent change in collection efficiency with increase in gas velocity from 15.5 to 89 cm/sec. However, at a gas velocity of 130 cm/sec the collection of the bed decreased by 10-15%. This is attributed to re-entrainment of deposited particles at high gas velocities.

5. Effect of Aerosol Concentration on Collection Efficiency

Figure 17 shows the effect of aerosol concentration on the collection efficiency of the thermal packed bed device. Varying the concentration from 1-125 μ $PbCl_2$/liter has no effect on the collection efficiency of the bed packed with 6 mm steel balls to a depth of 7.6 cm and gas velocity of 15.5 cm/sec. The collection efficiency is independent of aerosol concentration over all values of gas-packing temperature difference. Therefore, one may write

$$\frac{dC}{dt} = -Kc \qquad (7)$$

where

C = aerosol concentration, μg $PbCl_2$/liter

t = time, second

K = thermal deposition coefficient, $second^{-1}$
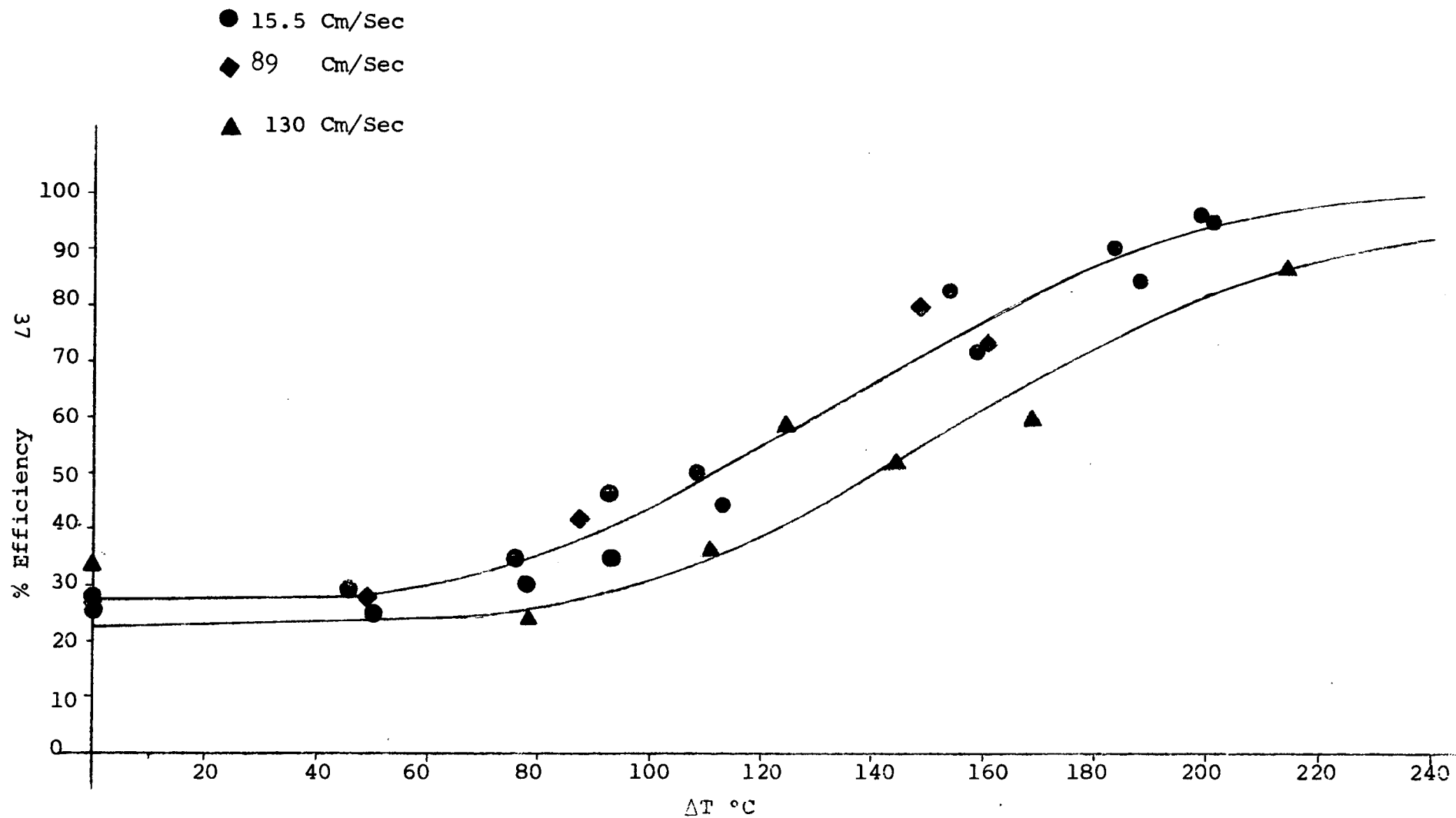
Figure 16 - Effect of Aerosol Flow Velocity on Collection Efficiency of the Thermal Bed
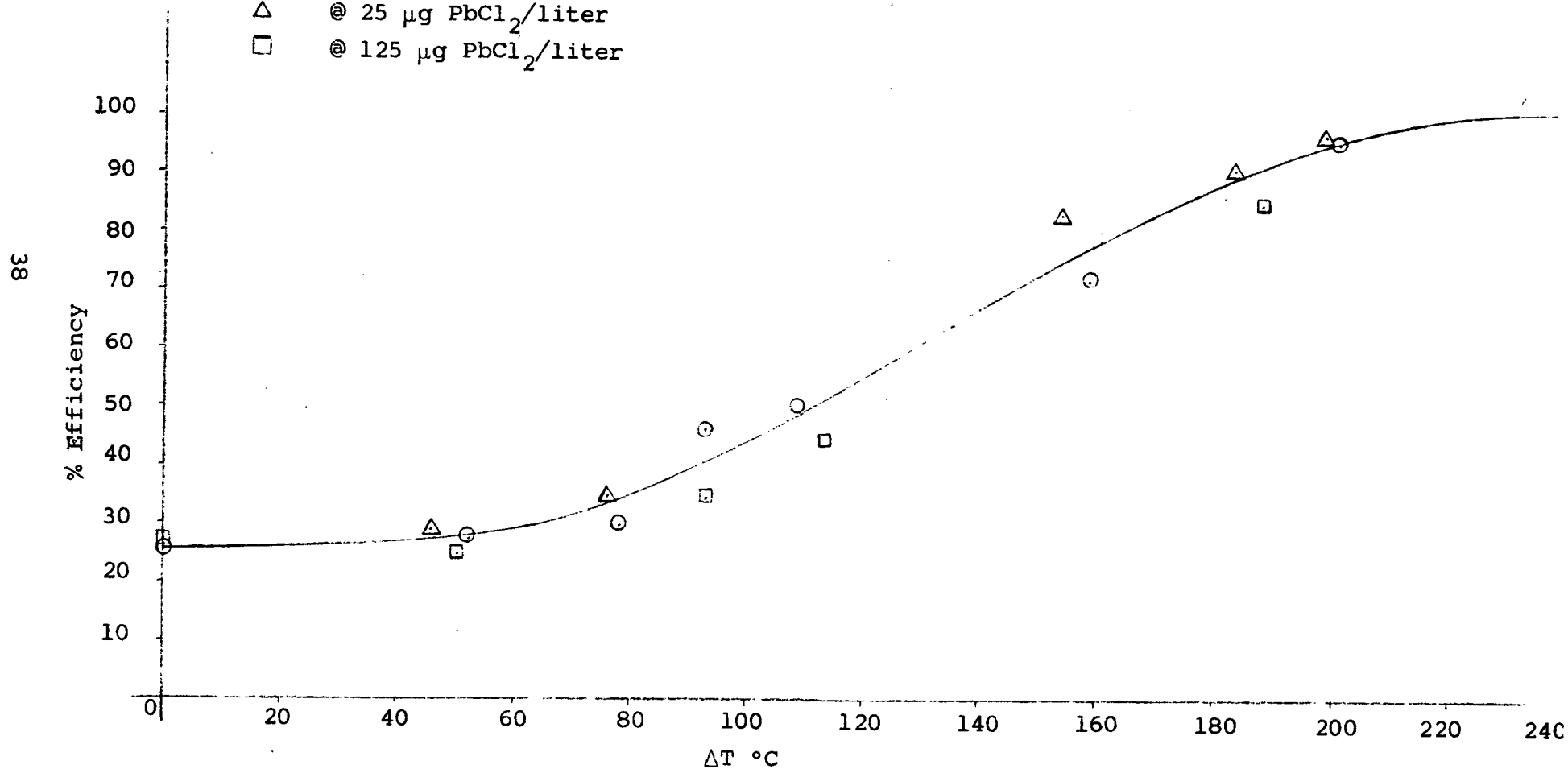
Figure 17 - Effect of Aerosol Concentration on Collection Efficiency of the Thermal Bed

The rate equation can be integrated to give

$$\ln \frac{C}{Co} = -Kt \qquad (8)$$

In the thermal packed bed device, K would be a function of ΔT essentially, because aerosol concentration, particle size, heat capacity of the packing and gas velocity have a negligible effect. At very high gas velocities, the particle deposition would decrease due to re-entrainment.

6. Effect of Contamination Build-Up on Collection Efficiency

The bed packed with 6 mm steel balls was contaminated with carbon soot from an oil lamp placed below the bed. The blower was left on to get an even coating of carbonaceous particles throughout the bed until visual examination showed that the bed had been contaminated quite heavily.

The heating characteristic of the contaminated bed has been plotted in Figure 14 which shows that the contaminated bed heats more slowly than the clean bed. The effect of carbon contamination on collection efficiency of the thermal packed bed device is shown in Figure 18. The collection efficiency of contaminated bed is higher than that of a clean bed. The contaminated bed is expected to have a higher surface area and rough packing surface. These effects would tend to increase the aerodynamic filtration efficiency of the bed.

Samples collected upstream and downstream of the contaminated bed were examined to see if any re-entrainment of contamination particles was taking place. There was no difference in the reflectance of the upstream and downstream samples. This confirmed that there was no significant dislodging of carbon particles. The filter samples were also examined with an optical microscope which showed there were very few carbon particles on the downstream samples. Photomicrographs shown in Figure 19 show
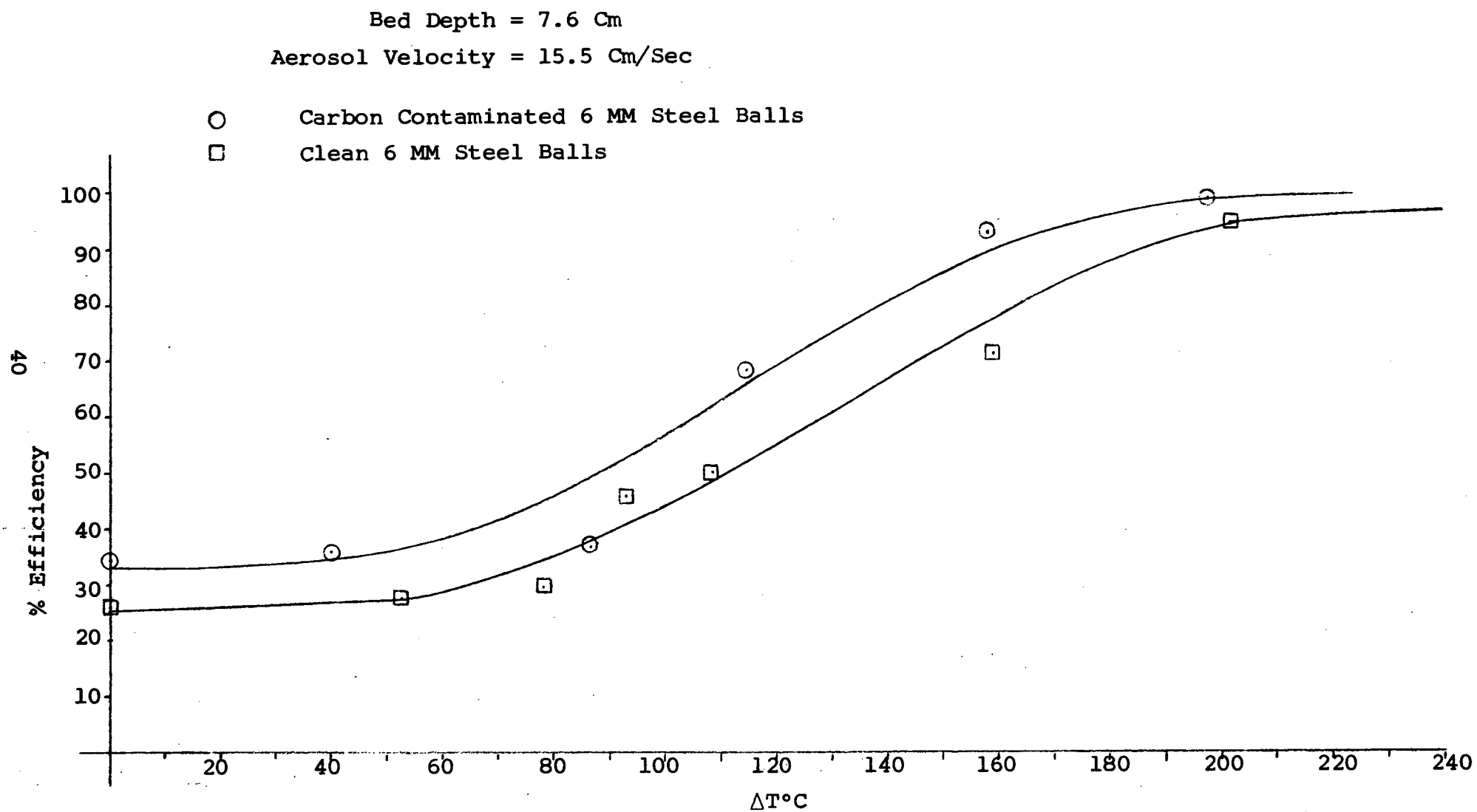
Figure 18 - Effect of Carbon Contamination on Collection Efficiency of the Thermal Bed
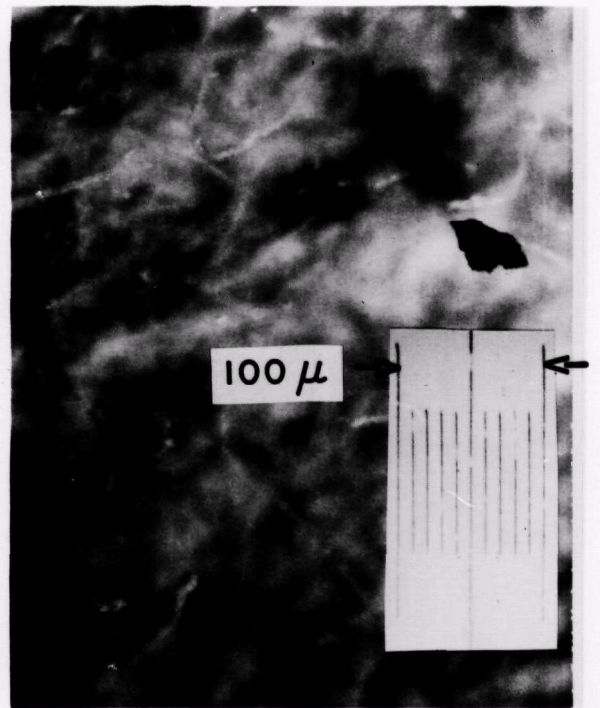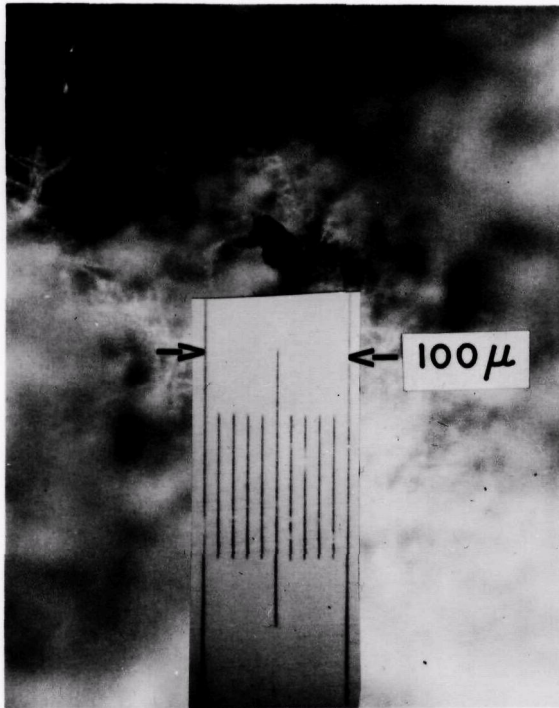
Figure 19 - Carbon Particles Coming Out of the Contaminated Bed

two such particles. It must be noted that the number of carbon particles dislodged was small and their size was greater than 10 μ. It is possible that large carbon particles dislodging from the bed would carry some lead particles that had deposited in the bed.

7. Effect of Gas-Packing Temperature Difference on Collection Efficiency

The gas-packing temperature difference, ΔT, is a measure of the thermal force which causes particles to move from a hot gas stream to the relatively cold packing surface. All the figures showing the effect of ΔT on the collection efficiency have a typical S shape. At small values of ΔT (<80°C), the thermal deposition is insignificant compared to aerodynamic capture of the particles, i.e., at low values of ΔT the packed bed essentially behaves as a coarse filter. However, as the gas-packing temperature difference increases thermal deposition starts contributing to the deposition processes and at high values of ΔT (>200°C) the packed bed attains an efficiency of nearly 100%. The overall efficiency E_O, of the packed bed device can be expressed as the sum of two efficiencies as

$$E_O = E_A + E_T \tag{9}$$

where

E_A = collection efficiency of the bed due to aerodynamic effects only = collection efficiency of the bed at $\Delta T = 0°C$.

E_T = collection efficiency of the bed due to thermal forces.

It should be noted that E_A would be independent of gas-packing temperature difference and E_T would primarily depend on the gas-packing temperature difference.

From Equation 8 we get

$$E_T = \frac{Co-C}{Co} = 1 - e^{-K\mathcal{T}} \tag{10}$$

where

K = thermal deposition coefficient, second^{-1}

$\mathcal{T}$ = particle residence time in the bed, second

$\mathcal{T}$ has a value of 0.2 seconds for a bed packed to 7.6 cm with 6 mm spheres at a gas velocity of 15.5 cm/second. Combining Equations 9 and 10, we get

$$E_O - E_A = 1 - e^{-K\mathcal{T}} \qquad (11)$$

The values of thermal deposition coefficient K have been calculated using equation 11 from the experimental values of E_O, E_A, $\mathcal{T}$ and ΔT. Figure 20 shows the effect of ΔT on thermal disposition coefficient K. The deposition coefficient is seen to increase very rapidly with the gas-packing temperature difference and approaches an asymptotic value at $\Delta T > 200°C$ which corresponds to virtually a 100% collection efficiency.

D. Compatibility of the Thermal Packed Bed Device with Automotive Systems

Experimental results in the preceeding section show that the most important variable affecting the collection efficiency of the thermal packed bed device is the gas-packing temperature difference. It is essential to maintain temperature differentials in excess of 200°C to operate the device with nearly 100% efficiency. Aerosol concentration and particle size have been found to have no significant effect on the performance of the device. Experimental results also show that the thermal packed bed device can be operated with high collection efficiency at gas velocities in the range 15 - 100 cm/sec. These experimental findings show that the mechanism of thermal deposition can be exploited by allowing the hot exhaust gases to flow past a cold packed bed maintaining a high temperature gradient.

It is essential that the thermal packed bed device be located downstream of the manifold where the exhaust gas temperature difference would be sufficient to insure virtually 100% collection.
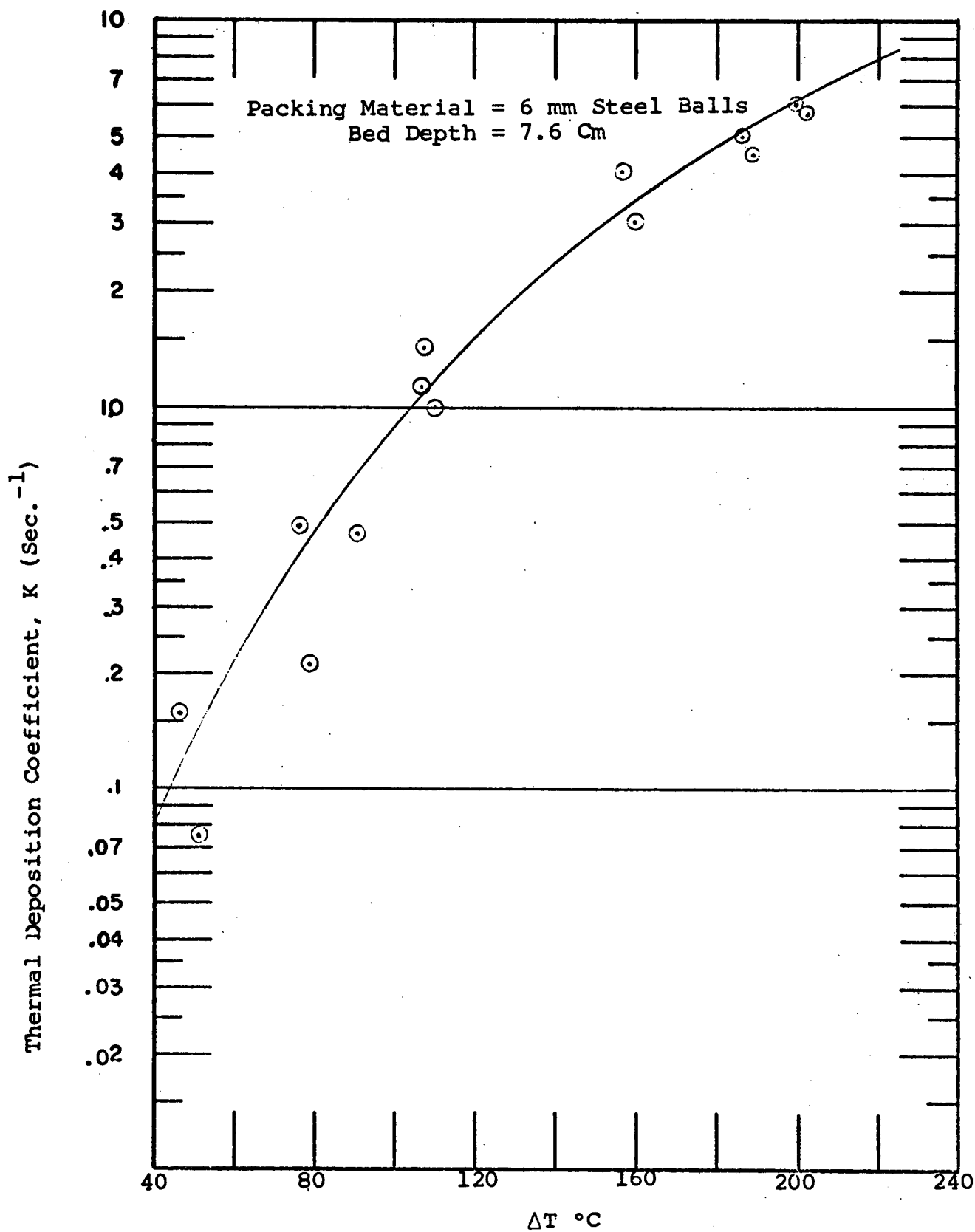
Figure 20 – Effect of Gas-Packing Temperature Difference
on Thermal Deposition Coefficient

Moreover, the vapor pressure of lead compounds at 300°C is low (0.001 mm Hg) and most of the lead in exhaust gas is in the particulate form. Under these conditions one can calculate the size of the packed bed device needed to process automobile exhaust as follows:

Exhaust rate (at standard conditions) = 9-95 l/sec (Ref. 1)
Operating temperature   = 250°C
Exhaust rate (at operating conditions) = 17-182 l/sec

It is reasonable to assume that the maximum permissible superficial gas velocity through the bed is 100 cm/sec. Then D_b, the diameter of the thermal packed bed device, can be calculated from

$$D_b = \sqrt{\frac{4Q}{\pi V_s}} \tag{12}$$

where Q is the exhaust rate in cm^3/sec and V_s is the superficial gas velocity through the bed in cm/sec. Substituting for Q and V_s in Equation 12 we get

$$D_b = \sqrt{\frac{4 \times 182,000}{\pi \times 100}} = 48 \text{ cm}$$

Therefore, a packed bed at least 48 cm in diameter would be needed to process the maximum exhaust emissions from an automobile engine. At the other extreme, where the exhaust rate is low (17 l/sec), the gas velocity through a 48 cm diameter bed would be approximately 9.5 cm/sec. The thermal packed bed device should be very effective at a low gas velocity of 9.5 cm/sec, since the residence time, $\mathcal{T}$, of exhaust gas in the bed would be large. The product $K\mathcal{T}$ in Equation 11 would also be large, increasing the collection efficiency of the device. Therefore, a 48 cm diameter bed could be packed to a height of about 8 cm with a suitable packing material to obtain a high collection efficiency with moderate pressure drop. The packing material should have a high surface area to volume ratio and the heat capacity of the bed would have to be quite large to maintain a high gas-packing

temperature differential for a long period. It is possible to use metal turnings or a fine packing material with high surface to volume ratio. The optimum size and shape of the packing material would have to be ultimately balanced against the maximum permissible pressure drop in the bed, which increases rapidly with increase in surface to volume ratio of the packing. Moreover, since the bed would heat with time on the passage of hot exhaust gases, a technique needs to be devised to permit the operation of the device maintaining a large gas-packing temperature differential all the time. One method for accomplishing this desired result in an automotive application is shown schematically in Figure 21.

Two packed beds would be used intermittently to clean the gas. As the exhaust gas flows through bed B, bed A is cooled by a flow of relatively cold outside air. When the temperature sensor above bed B indicates that the bed is too warm to operate efficiently the butterfly valve changes to channel the flow to the second bed A.

An alternate approach would be to cool the bed internally. If a suitable technique could be devised for internal cooling of the bed, then only one packed bed would be required to collect particles from auto exhausts with a high collection efficiency. In time, the beds could accumulate enough carbon and other deposits to impede the flow, and maintenance could be required. However, this may involve simply dumping the packing and replacing with fresh packing, probably some cheap material such as sand or gravel.
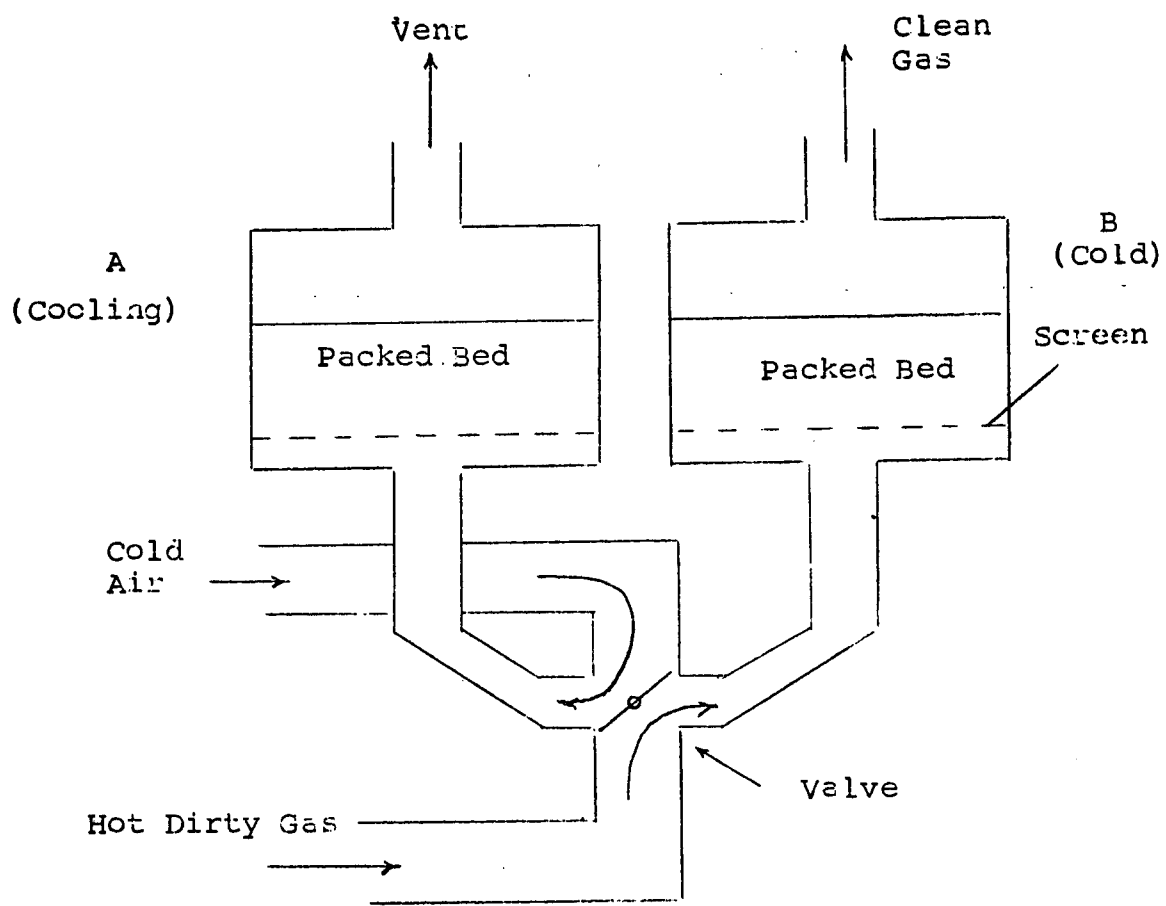
Figure 21

Packed Beds For Collection of Submicron
Particles by Thermal Precipitation

IV. SONIC FLUIDIZED BED DEVICE

Aerosols in the submicron size range which cannot be conveniently collected can sometimes be coagulated to form agglomerates which are more easily separated. Coagulation can occur naturally by Brownian motion or can be induced by sonic waves or turbulence. Brownian coagulation has been shown to proceed according to the Smoluchowski equation

$$\frac{dn}{dt} = -Kn^2 \qquad (13)$$

where

n = aerosol concentration, particles/cm^3

t = time, second

K = Coagulation constant, cm^3/second

The Smoluchowski equation can be integrated to

$$\frac{1}{n} - \frac{1}{n_o} = K\,t \qquad (14)$$

where n is the final concentration and n_o is the original concentration of aerosol. In order to "grow" 0.1 micron particles to 1000 times the mass, the equivalent of a one micron particle, long times are required. The coagulation constant is in the order of 7×10^{-10} (Ref. 16). Therefore,

$$\frac{1000}{n_o} - \frac{1}{n_o} = 7 \times 10^{-10}\,t$$

$$t = \frac{999 \times 10^{10}}{n_o \times 7} = \frac{1.42 \times 10^{12}}{n_o}$$

Thus, unless the original particle concentration were in order of 10^{12} particles per cm^3, Brownian coagulation cannot be expected to achieve sufficient growth of the aerosol particles in short enough time to enable collection by inertial devices.

High frequency sound waves have been demonstrated to accelerate coagulation of aerosols. For example, Stokes (Ref. 18)

reported that carbon black smoke which had a primary particle size of 0.05 micron could be coagulated with sound frequencies of 4000 cycles per second. Sonic agglomeration follows the relationship (Ref. 19,20).

$$n = n_o \exp - Kt \qquad (15)$$

where n is the particle count, n_o is the original particle count, and K is the coagulation coefficient. Again to "grow" the particles by a factor of 1000

$$\frac{1}{1000} = \exp - Kt$$

$$- Kt = - 6.9$$

and for a holding time of 1 second a K of 6.9 would be required. Brandt (Ref. 19) reports a K of 1.28 at a sonic flux of 0.1 watts/cm^2. Since K varies as the square root of the power flux, a power flux of 4.7 watts per square centimeter would be required to achieve the necessary coagulation rate. This would be equivalent to approximately 6 horsepower for one square foot of agglomeration chamber. This power level would have to be reduced for a practical device, possibly by increasing the number of coagulation centers (Ref. 21), i.e., large particles which sweep the smaller particles under the influence of sonic vibration. This phenomenon has been demonstrated and reported in the literature (Ref. 22). Water sprays were shown to increase the coagulation rate of carbon smokes in a sonic field. Thus, it is reasonable to expect that in a dense system such as a fluidized bed (Ref. 16) where the distance between particles is small, high deposition rates of the submicron particles onto the larger fluidized particles would occur. The sonic waves cannot be expected to penetrate deeply into the bed. However, absorption of sonic energy is a direct result of particle motion which is the desired effect.

The second technique studied to control particle emissions from auto exhausts was the fluidized bed. The mechanism of aerosol removal in fluidized beds is related to the high velocity gradients in a gas flow around the particles in the bed. The aerosol particles do not follow the flow stream lines because of their inertia and impact on the fluidized bed particles, adjering to them. The velocity gradients between the bed and aerosol particles can be enhanced by superimposing a sound field. Moreover, the ratio of the amplitude of vibration of submicron aerosol particles to the amplitude of the sound motion to which they are subjected is very nearly unity. Therefore, in the presence of sound waves, the effective particle size along the axis of vibration becomes larger, increasing the probability of collision between the bed and the aerosol particles.

A. Collection Efficiency of Fluidized Bed Without Sonic Enhancement

The effectiveness of a 3.8 cm diameter fluidized bed for removing submicron lead particles from an air stream was investigated at superficial gas velocities of 15-60 cm/second. The aerosol stream from the generator was diluted to give approximately 50 μg $PbCl_2$/liter. The diluted aerosol stream was used to fluidize the bed. Simultaneous aerosol samples were collected both upstream and downstream of the bed.

Initial tests, with 74-149 μ sand particles as the fluidized material, showed that there was considerable attrition of the sand particles on fluidization resulting in carry-over of the fine material. Therefore, it was decided to fluidize 210-500 μ glass beads and study the effect of superficial gas velocity on the collection efficiency of the bed.

The experimental results on collection efficiency of the fluidized bed device without any sonic enhancement is shown in Figure 22. The collection efficiency decreases rapidly with increasing superficial velocity. This is because at low flow
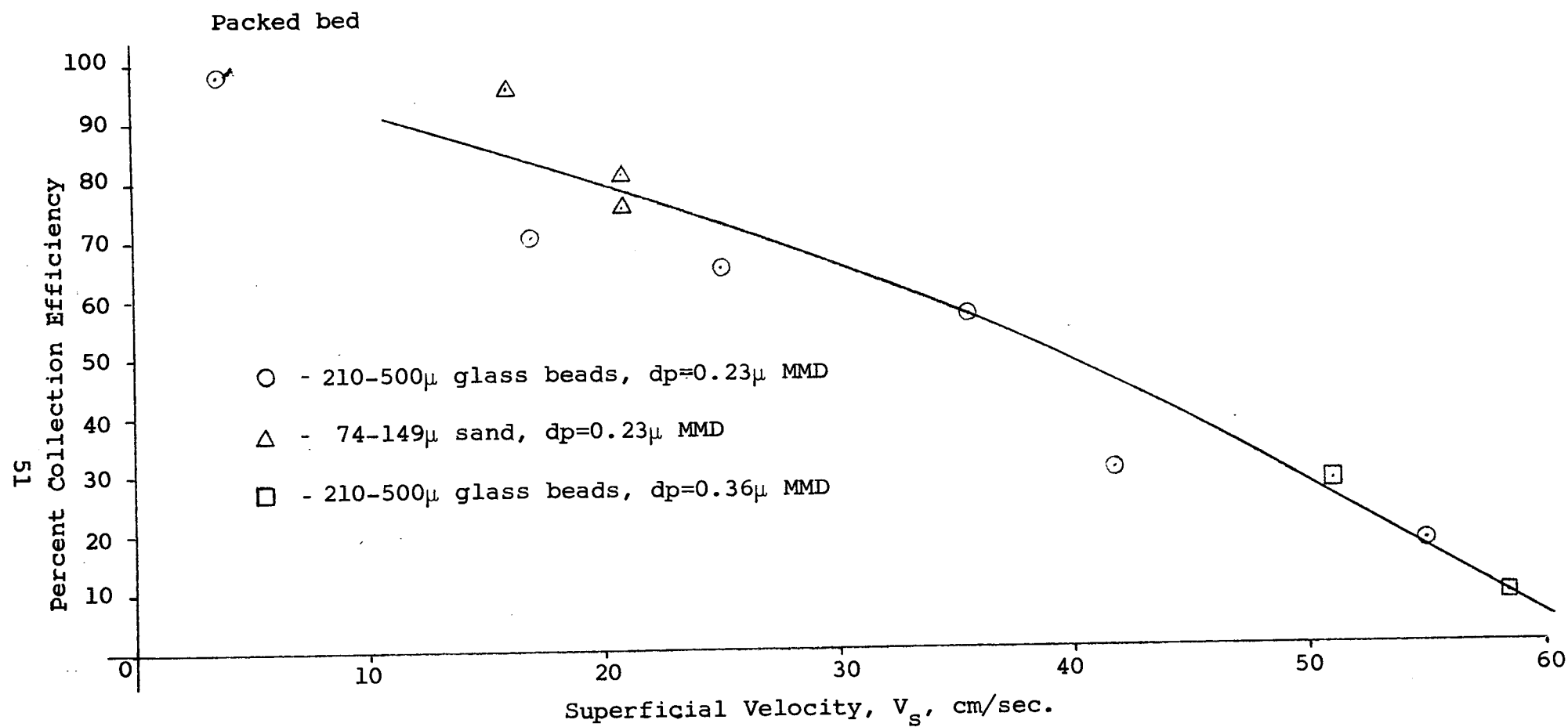
Figure 22 – Effect of Superficial Velocity on Collection Efficiency of Fluidized Bed Without Sonic Enhancement

velocities, the bed essentially behaves as a coarse filter more than compensating for its large pore size by its thickness. At higher flow velocities the bed starts "boiling" and its filtration effectiveness is considerably lessened. Figure 22 also shows that there is no significant effect of particle size in the range 0.2-0.4 μ on collection efficiency.

B. Enhancement of Collection Efficiency of Fluidized Beds with Sonic Techniques

1. Theory

Sonic energy has been noted to enhance the filtering efficiency of packed beds, (Ref. 23), but questions remain on the optimum values of frequency and amplitude and the relative merits of sonic energy as compared to larger or deeper beds. In the application in mind at this time, i.e., increase in collection efficiency of particulates from automobile exhaust by a fluidized bed with sound, sonic energy is very desirable because of the space and mass limitations.

The hypothesis is that the effectiveness of sound energy in increasing the collection of aerosol particles depends on the oscillatory motion of the aerosol particles in the sound field. The fact that the pressure also fluctuates is believed to have no bearing on the problem. If the hypothesis as stated is correct, we expect to find that the sonic energy must be such that the velocity amplitude of the sound wave must be at least of the same order as the steady flow velocity through the bed. This velocity will then appear as something like a threshold and there will be no effect of sound for all amplitudes significantly below this level. Also, if the displacement amplitude of the particles in the sound wave exceeds the depth of the bed further increases in amplitude will have smaller effects.

In order to test the hypothesis, experiments were conducted to determine the acoustic particle velocity in the bed, using the experimental set-up shown in Figure 23. Direct measurements of the velocity amplitude were not possible, therefore, it was
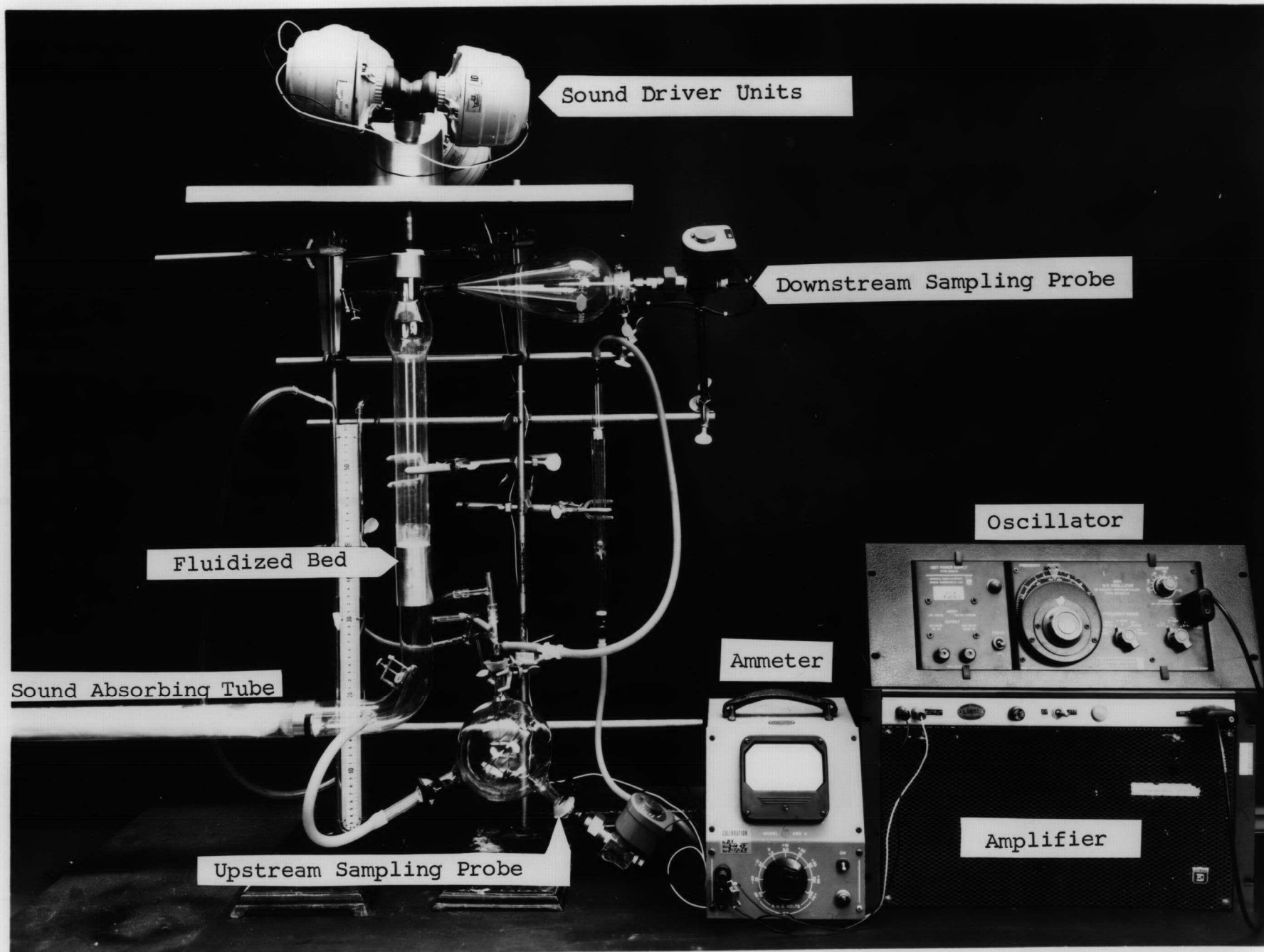
Figure 23 - Experimental Setup with Travelling Waves

necessary to measure pressure and standing wave ratios and compute the amplitude transmitted into the bed. Precision of measurement of the relative quantities was impaired by the large fluctuations in the bed properties due to breaking up of individual gas bubbles during fluidization.

The velocity amplitude, V, is related to the acoustic pressure, P, (as measured with a microphone) in a traveling wave when there are no reflections through the acoustic impedance, Z, of the medium by the ratio:

$$P/V = Z = \rho C \tag{16}$$

where ρ is the density and C the sound velocity in the medium. The velocity amplitude in the bed was computed from the pressure amplitude of the wave above it. The following observations permitted computations to be simplified.

(a) With no flow through the bed, the bed behaved like a rigid wall and the pressure minima were exactly one quarter wavelength from the surface of the bed.

(b) When air flow was introduced, the pressure level at the minima increased but their position was not greatly affected.

(c) The attenuation of the pressure amplitude in the bed itself was sufficiently large so that reflections from the lower end of the bed could be neglected. This observation was further corroborated by the additional observation that the phase change within the bed was uniform with distance in contrast to the step-like phase transitions at the minima of the standing wave above the bed.

The following argument is used to compute the velocity amplitude, V_t, transmitted into the bed from the pressure maxima, P_m, and the pressure minima, P_n, in the standing wave in front of the bed. The standing wave in front of the bed is made up of the incident wave P_i and the reflected wave, P_r. The corresponding velocity amplitudes, V, are designated with the same subscripts. Then:

$$P_i/V_i = -P_r/V_r = Z_a \qquad (17)$$

$$P_t/V_t = Z_b \qquad (18)$$

$$P_i + P_r = P_m \text{ and } P_i - P_r = P_n \qquad (19)$$

$$V_t = V_i + V_r \qquad (20)$$

$$= \frac{P_i}{Z_a} - \frac{P_r}{Z_a} = \frac{P_n}{Z_a}$$

where Z_a is the impedance of the air above the bed and Z_b is the impedance of the bed itself. Thus, the velocity amplitude of the sound wave traveling into the bed immediately below the surface of the bed is $V_{to} = P_n/Z_a$. At greater depths, the velocity amplitude deminishes through the attentuation factor, α:

$$V_{tx} = V_{to} e^{-\alpha x} \qquad (21)$$

In derivation of Equation 21, variation of velocity amplitude with bed depth x has been assumed to be identical to the variation of the pressure amplitude by neglecting additional reflections from the base of the bed. The high attenuation in the bed, in nearly all cases, minimizes errors due to this assumption.

2. Determination of Acoustic Particle Velocity

The parameter of greatest interest is the acoustic particle velocity, V_p, in the sound wave. The parameter cannot be measured directly. It is only possible to measure the acoustic pressure and infer the particle velocity from the impedance of the medium.

The impedance of the medium was determined from the standing wave pattern in the tube above the bed itself. A 3 mm diameter probe tube permitted measurement of the sound pressure at any point in the bed. The probe tube attenuation was determined by

comparison with the output of a microphone mounted in the wall of the tube containing the bed at different frequencies from Figure 24.

The velocity amplitude was subsequently related to the current in the loud speaker voice coils eliminating the need for a microphone, probe tube and auxilliary equipment during actual experiments with lead aerosols.

The microphone output was found to vary by less than $\pm$ 3dB at any frequency at different locations above the screen as shown in Figure 25. The effect of sound frequency and gas velocity on particle velocity, V_p, was calculated from the maximum and minimum sound pressure levels in front of the bed at a constant current input to the voice coils of the speakers. The ratio of particle velocity to current input, A, to the speakers has been plotted in Figure 26 for traveling sound waves.

In the case of standing waves, the particle velocity was computed from the relationship

$$V_{p\ max} = P_{max}/\rho C \qquad (22)$$

where $V_{p\ max}$ is the maximum particle velocity. It must be noted that in order to attain maximum particle velocity, the bed must be positioned at a pressure minimum of the sound wave. At room temperature, the density of air is 1.2×10^{-3} gm/cm^3 and the velocity of sound is 3.44×10^4 cm/sec. Therefore, the acoustic impedance, ρC, of air at room temperature is 41.3 gm/cm^2 second. Equation 22 then becomes

$$V_{p\ max} = P_{max}/41.3 \qquad (23)$$

The maximum particle velocity was calculated using Equation 23 from the maximum sound pressure level, P_{max}, (measured by a microphone) at different current inputs to the sound driver units. At a gas velocity of 29 cm/sec and frequency of 660 Hz, P_{max} was found to be 146 dB and 156 dB at current inputs of
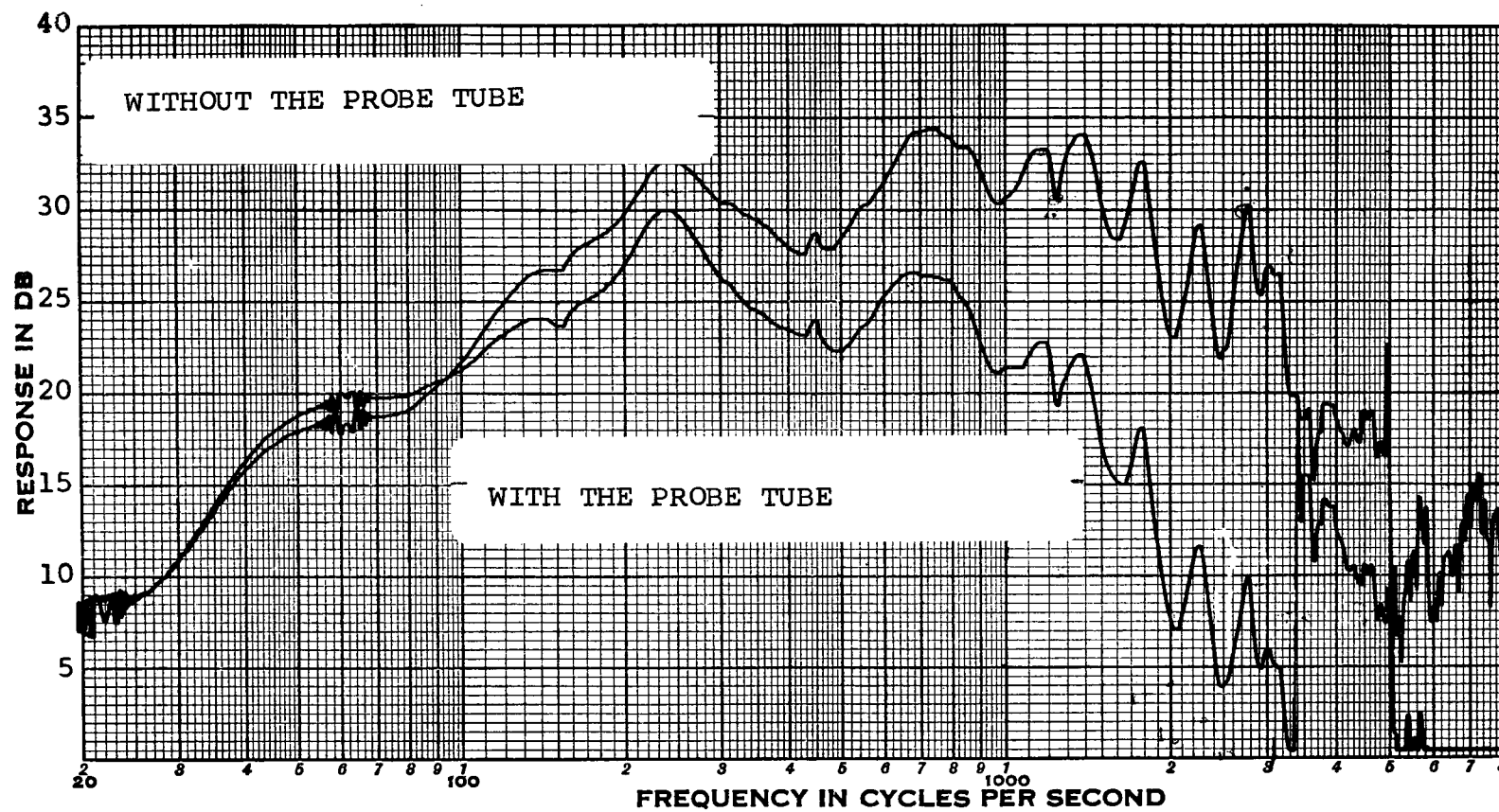
Figure 24

Difference in Sound Pressure Levels when
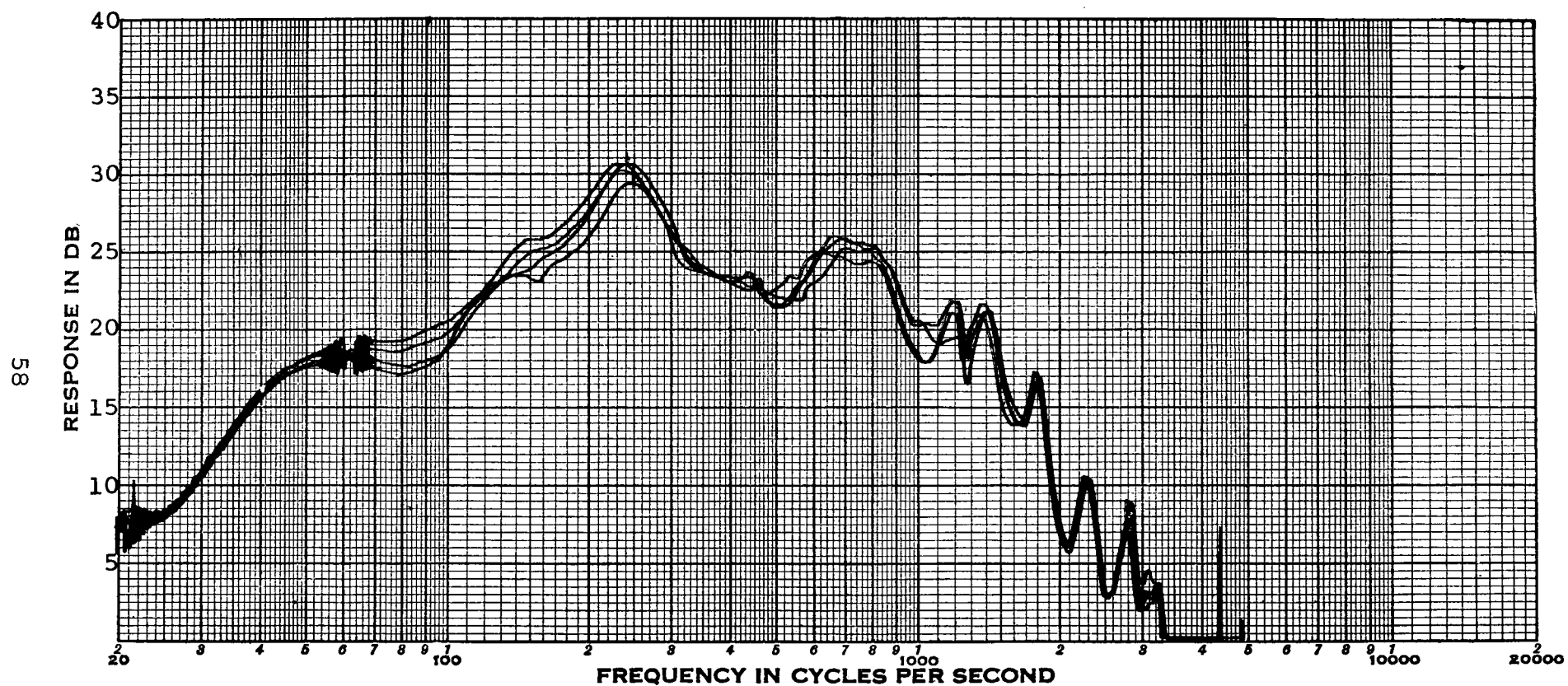Measured with and without the Probe Tube

Figure 25

Sound Pressure Levels as a Function of
Frequency at the Retaining Screen, 10, 20 and
26 cm. above the screen (No Bed Present)
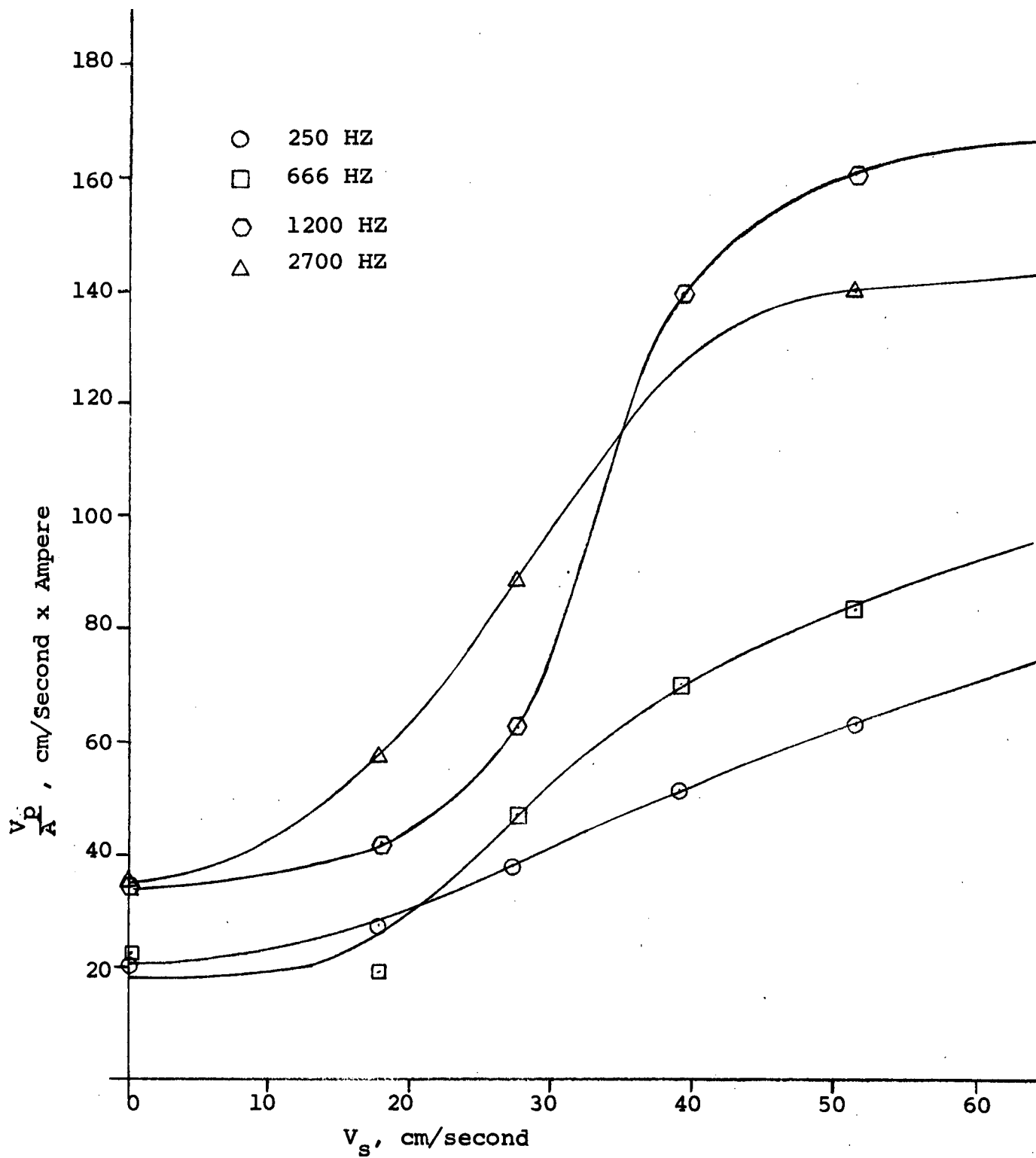
Figure 26 - Effect of Flow Velocity and Frequency of Sound on V_p/A

0.315 and 1 ampere respectively. Using these values in Equation
23, we get:

$$\frac{V_{p\ max}}{A} = 305\ \frac{cm}{sec\ x\ ampere} \tag{24}$$

C.   Effect of Traveling Sound Waves on Collection Efficiency of the Fluidized Bed

Figure 23 shows the experimental set-up to determine the
effect of traveling sound waves on the collection efficiency of
the fluidized bed. The 3.8 cm diameter bed was filled to a
depth of 5 cm with 210-500 μ glass beads. A small stream of
aerosol from the aerosol generator was mixed with a stream of
dry filtered air in a chamber. The aerosol concentration and
flow rate could be varied by adjusting the two streams and the
mixed stream was used to fluidize the bed. Simultaneous aerosol
samples were obtained both upstream and downstream of the fluidized
bed as shown in Figure 23.

A speaker bank was assembled by connecting four University
Model ID-60 driver units* in parallel and mounted on top of the
fluidized bed so that the sound waves traveled down the
fluidization chamber. The speaker bank was connected to a
frequency oscillator type NO1210-C** through a 400 watt amplifier
and an ammeter. A 1.2 meter tube packed with fiberglass was
connected to the bottom of the fluidized bed. The packed tube
served as a sound absorber to give near ideal traveling sound
waves within the fluidized bed device.

A series of experiments were performed to study the effect
of sound frequency and power input to the speakers on the
collection efficiency of the bed. The experimental data on the
collection efficiency of the fluidized bed device with traveling
sound waves is given in Table V.

---

 * Manufactured by Altec Electronics, White Plaines, N.Y.
**Manufactured by General Radio Co., Concord, Massachusetts

Table V

EXPERIMENTAL RESULTS WITH TRAVELING SOUND WAVES

Aerosol Size, dp = 0.34 μ MMD
Bed Height   = 5 cm
Bed Diameter   = 3.8 cm
Bed Material   = 210-500 μ glass beads
Gas Velocity, V_s = 29 cm/sec

Current to, Sound Drivers, Amperes	Frequency, HZ	Aerosol Concentration, μg PbCl$_2$/lit	V_p/A	V_p	% Collection Efficiency
0.3	2700	44.3	94.5	28.4	32.6
1.0	2700	50.6	94.5	94.5	13.4
1.5	2700	35.7	94.5	141.8	25.1
2.0	2700	43.5	94.5	189	23.2
2.5	2700	55.2	94.5	236	30.4
3	2700	24.9	94.5	283	39.3
0.3	1200	66.6	70	21	21.8
1.0	1200	46.4	70	70	30.4
1.5	1200	49.9	70	105	37.5
2.0	1200	77.4	70	140	40.8
2.5	1200	60.1	70	175	32.8
3	1200	61.4	70	210	29.6
0.3	660	83.7	50.5	15.1	38.1
1.5	660	65.6	50.5	75	40.5
3.0	660	50.8	50.5	150	42.5
0.3	250	24.9	40.0	12.	43.5
1.5	250	81.4	40.0	60	37.9
3.0	250	81.4	40.0	120	31.8

1. Effect of Sound Frequency on Collection Efficiency

The effect of sound frequency, in the range 250-2700 HZ, on the collection efficiency of the fluidized bed with traveling sound waves is shown in Figure 27. This frequency range corresponds to high values of sound pressure levels in the bed as shown in Figure 24 and should be more effective than other frequencies. Figure 27 shows that there is no systematic change in collection efficiency of the bed with frequency at any power input to the sound driver unit. Some energy is lost through mechanical friction, and eddy currents in the electromagnetically driven diaphragm type sound driver units. Moreover, some energy is also absorbed by the bed. Since all these energy losses vary with frequency, it is not surprising that there is no pattern on the effect of frequency on collection efficiency of the bed.

2. Effect of Particle Velocity on Collection Efficiency

Particle velocity, V_p was determined using Figure 26 from known values of sound frequency, gas velocity and current input to the speakers. Figure 28 shows the effect of particle velocity on collection efficiency of the bed. Since V_p is a function of frequency, gas velocity and current to the speakers, the collection efficiency should be a function of the particle velocity alone even though the other parameters were varied. Figure 28 shows that even at high particle velocities of 200- 300 cm/sec there is no significant increase in the collection efficiency of the bed. Collection efficiency values of 30-40% indicate that traveling sound waves are very ineffective and do not enhance the collection efficiency of the fluidized bed.

D. Effect of Standing Sound Waves on Collection Efficiency of the Fluidized Bed

The experimental set-up to study the effect of standing sound waves on collection efficiency of the fluidized bed is
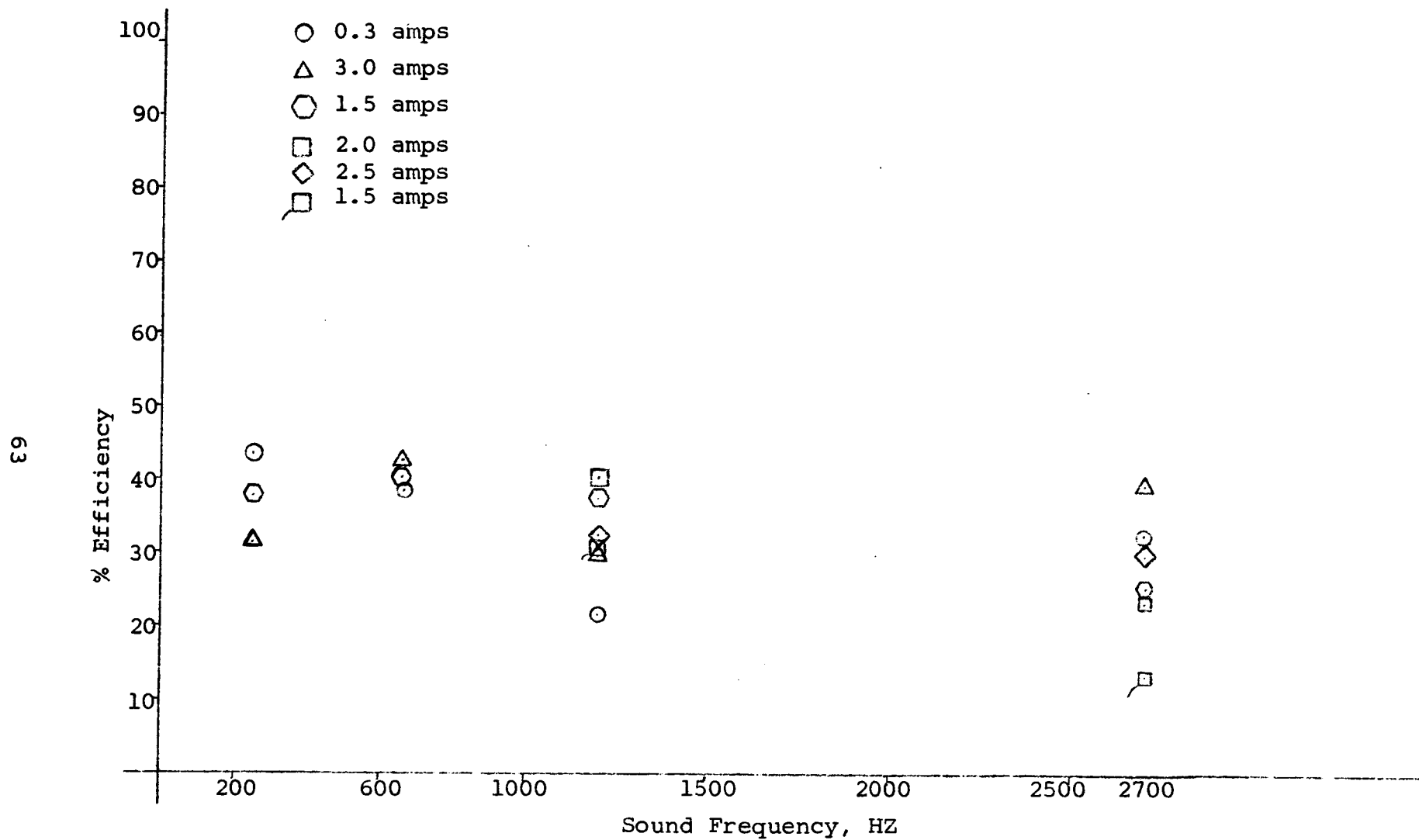
Figure 27 – Effect of Sound Frequency on Collection Efficiency of the Fluidized Bed with Travelling Waves
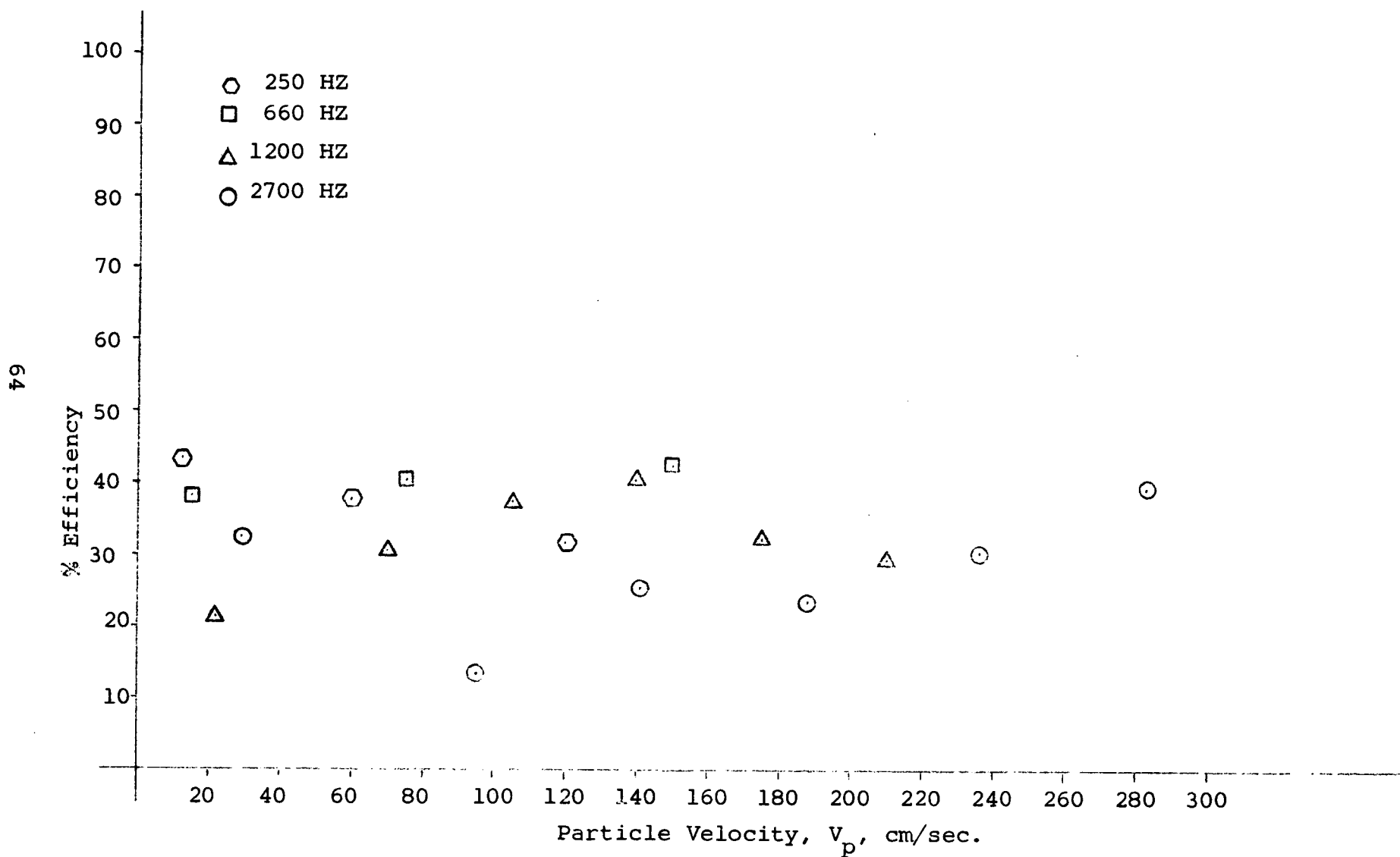
Figure 28 – Effect of Particle Velocity on Collection Efficiency of the Fluidized Bed with Travelling Waves

shown in Figure 29. The aerosol generation, sampling and flow system were the same as in the case of traveling waves. The fiber glass packed sound absorbing tube was removed and the fluidized bed device was modified to get standing wave patterns in the bed.

The system consisted essentially of three nested glass tubes sealed with rubber rings and provided with a screen to support the fluidized bed. The sound source, consisting of four loud speaker driver units (University ID-60), was mounted above the bed and connected to the fluidized bed unit with a short section of brass pipe as shown in Figure 30.

The nested tubes were required to tune the system which was essentially a closed pipe resonator. Ideally, maximum sound amplitude should occur at multiples of quarter wave lengths from the reflecting bottom of the tubes and the distance from the horn diaphragm to the bed should also be a multiple of quarter wave lengths for optimum effect of sound. The nested tube arrangement allowed adjustment of both the horn to bed and the reflector to bed distances.

The position of the bed was adjusted with respect to the sound driver units and the bottom of the reflector tube by noting the intensity of scattered light from the aerosol downstream of the bed. At the best location of the bed, the concentration of $PbCl_2$ aerosol particles downstream of the bed was small. This position of the bed coincides with the minimum pressure and maximum velocity level in the soundwave.

Figure 31 shows the effect of current input to the speakers on the collection efficiency at a frequency of 660 Hz and gas velocity of 29 cm/sec. It is seen that the collection efficiency of the fluidized bed increases rapidly with power input when standing sound waves were used.

The collection efficiency of the bed exceeds 90% at a current of 5.6 Amperes, which corresponds to an electrical power input of 125 watts, to the sound driver units. Because some

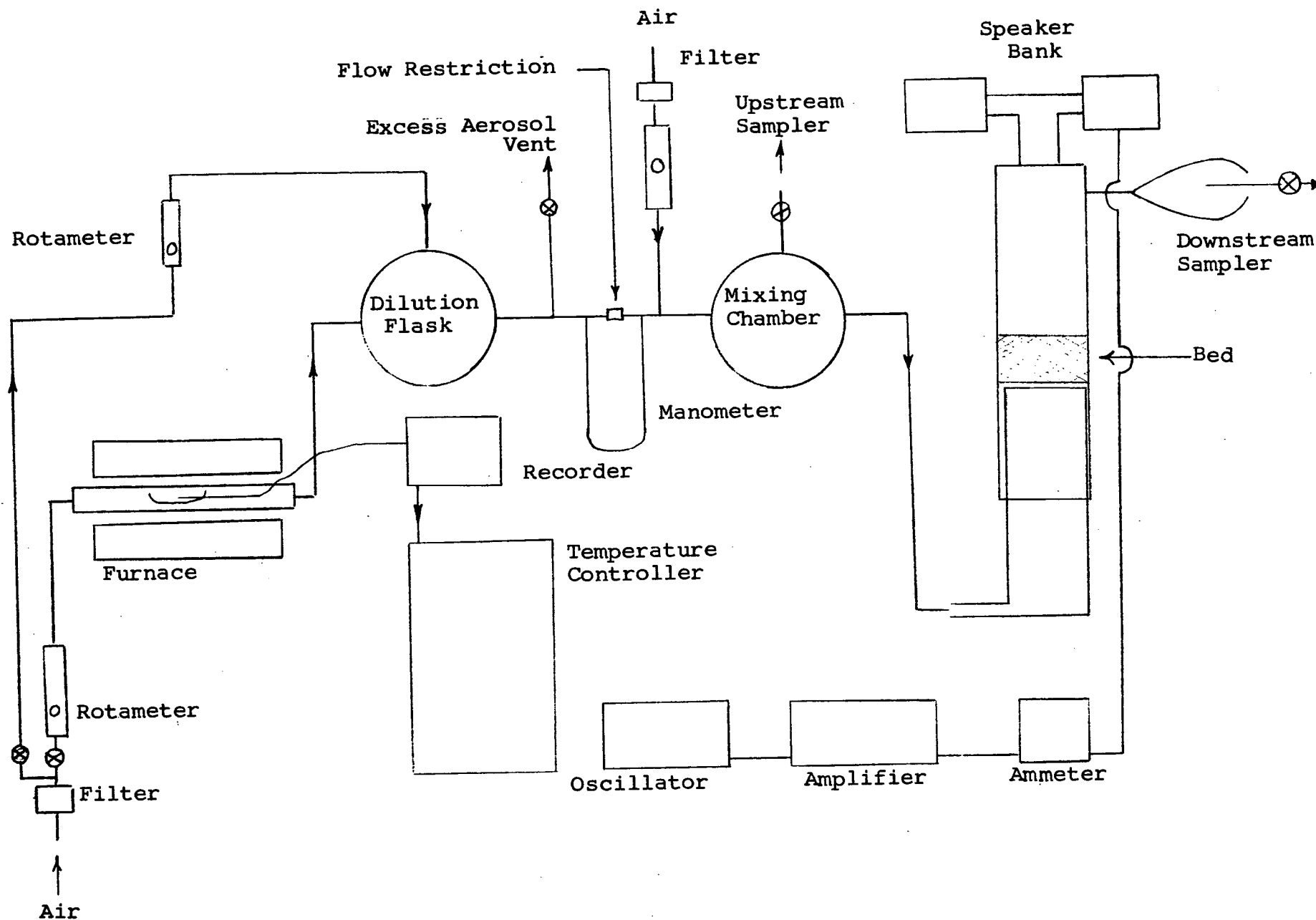Figure 29 - Experimental Setup to Study the Effect of Standing Sound Waves
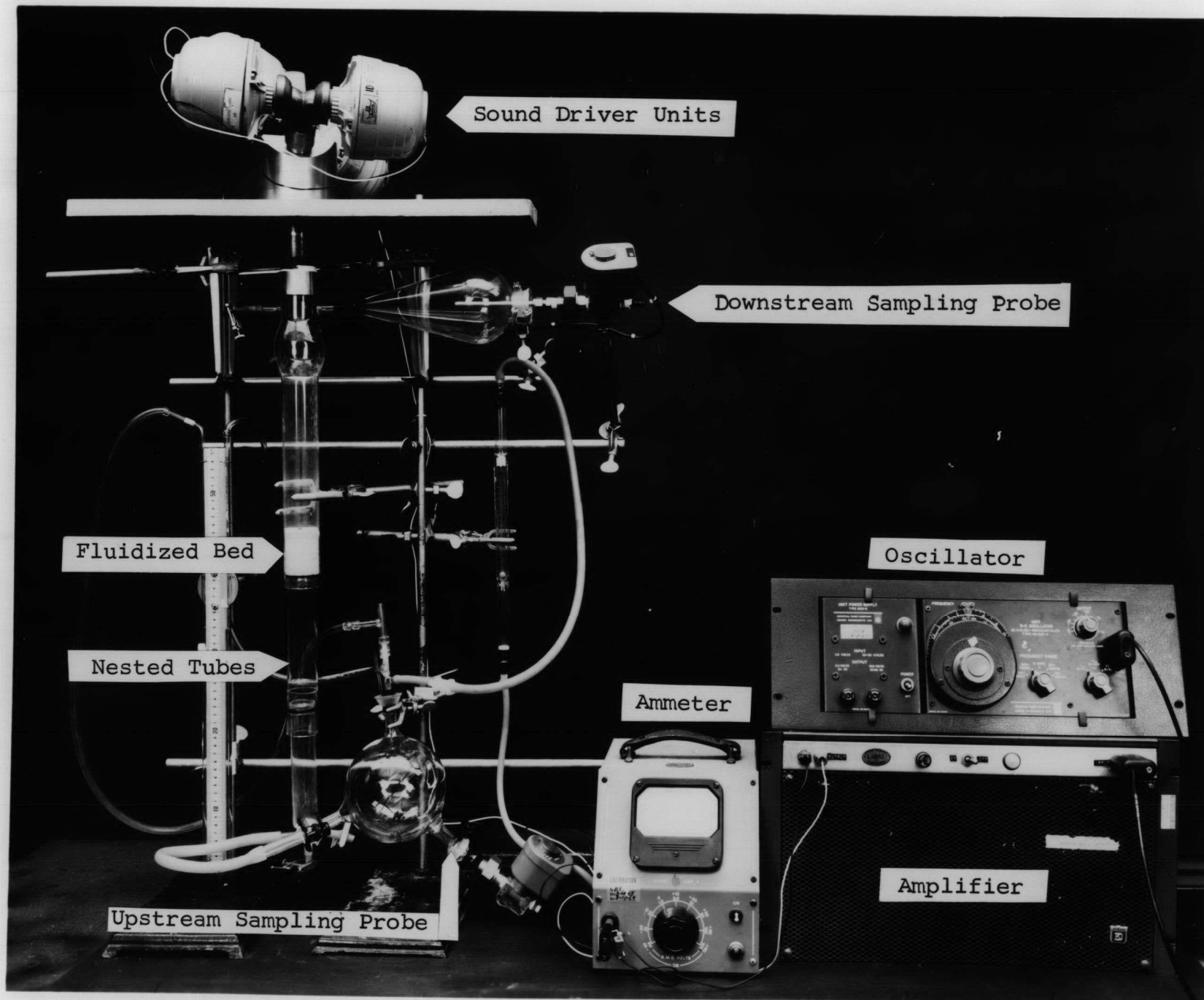
Figure 30 - Experimental Setup with Standing Waves

Frequency — 660 HZ
Aerosol Size — 0.34µ MMD
Bed Material — 210-500µ Glass Beads
Gas Velocity — 29 Cm/Sec.

% Efficiency

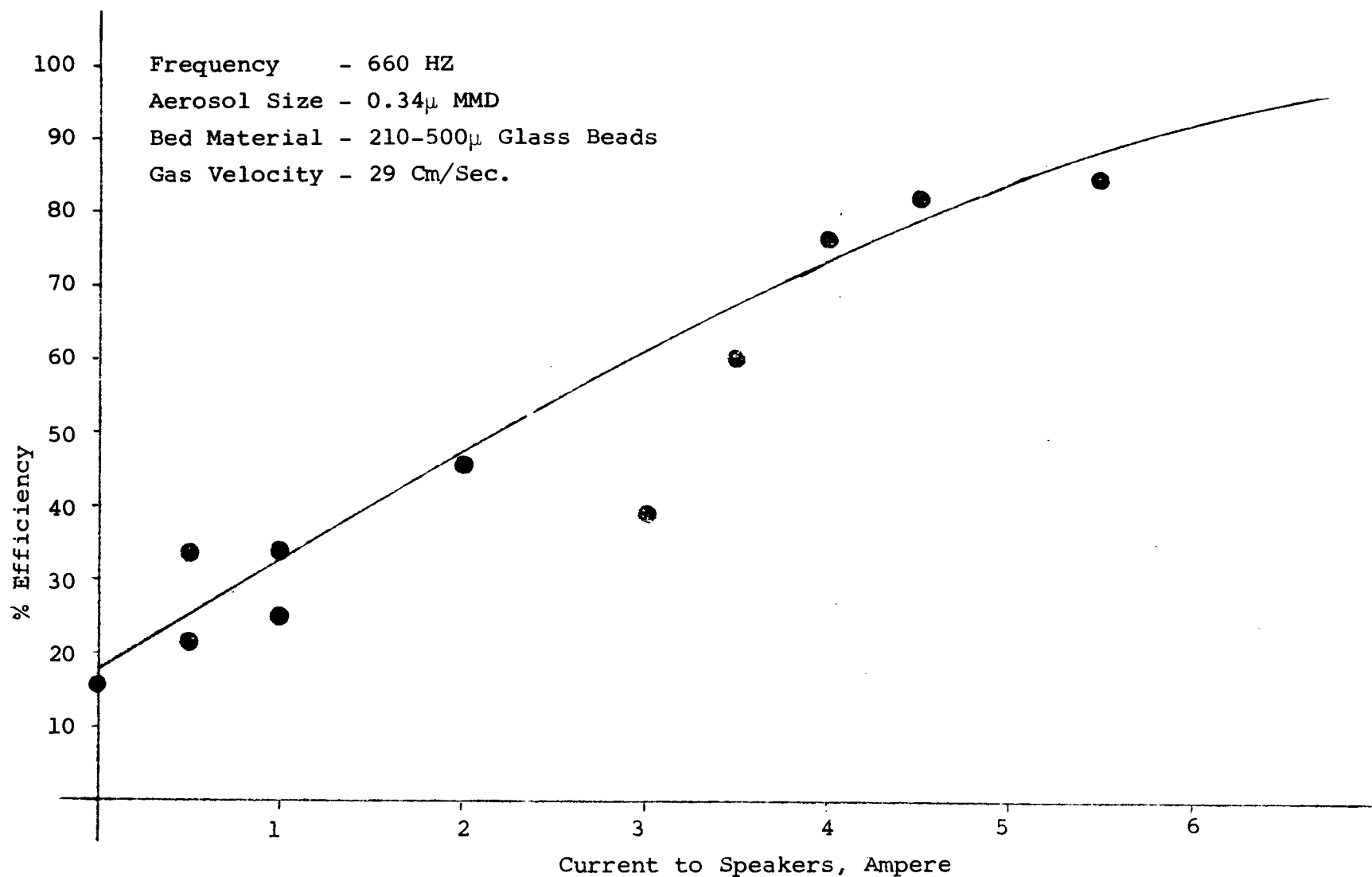Current to Speakers, Ampere

Figure 31 — Effect of Power Input to the Speakers on the Collection Efficiency of the Fluidized Bed with Standing Sound Waves

89

energy is lost due to mechanical friction and eddy current dissipation in the sound driver units, and by absorption in the bed itself, only a fraction of the electrical power input to the sound driver units would be effective as sound energy in the bed. It is reasonable to assume that approximately 5% of the power input to the speakers was converted to useful sonic energy. Then, the "active sonic flux", W, in the 3.8 cm diameter fluidized bed is:

$$W = \frac{125 \times 0.05}{\frac{\pi}{4} \times (3.8)^2} = 0.5 \text{ watts/cm}^2 \tag{25}$$

Therefore, it would be necessary to have a sonic flux of at least 0.5 watts/cm^2 in the bed for the sonic fluidized bed device to operate with an efficiency of 90%. It was not possible to conduct experiments at higher power inputs, with the driver units employed in the study, because of maximum power input limitations imposed by the design of the units.

The effect of particle velocity on collection efficiency of the sonic fluidized bed device is shown in Figure 32, both for traveling and standing sound waves. It is evident from the figure that at low values of particle velocity the collection efficiency is not affected by the particle velocity. The collection efficiency increases with particle velocity when the latter exceeds 500 cm/sec. This corroborates our original assumption that acoustic particle velocity must be significantly greater than the steady gas velocity through the bed. The higher values of collection efficiency of the bed with standing waves compared to traveling waves can be explained as follows:

From Figure 26, at gas velocity of 29 cm/sec and frequency of 666 Hz we get,

$$(V_p/A)_{\text{traveling waves}} = 50 \frac{\text{cm}}{\text{sec} \times \text{amp}} \tag{26}$$

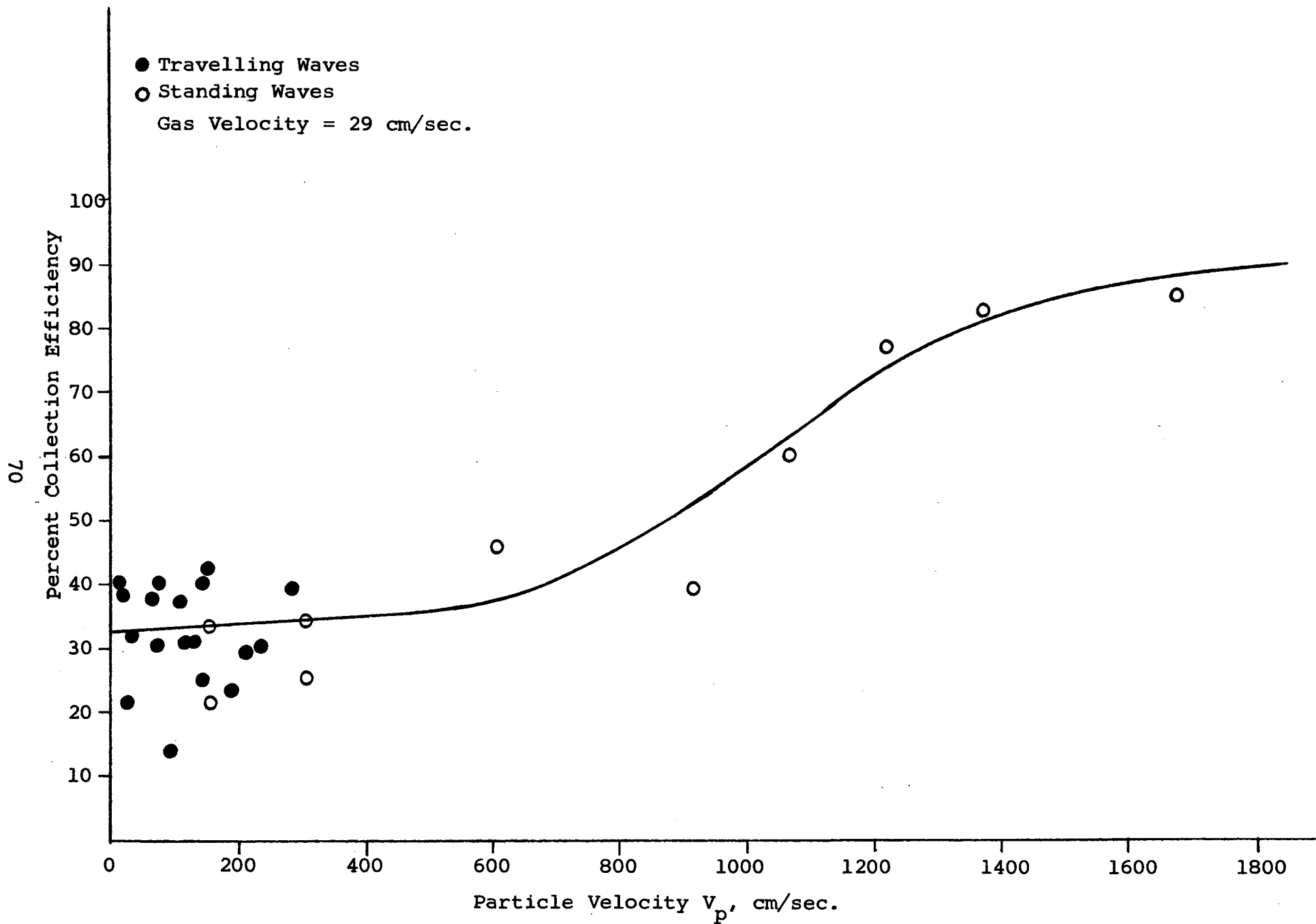For standing waves at gas velocity of 29 cm/sec and frequency of 660 Hz we get (see Equation 24),

Figure 32 – Effect of Particle Velocity on Collection Efficiency of the Sonic Fluidized
Bed Device

$$(V_{p\ max}/A) \text{ standing waves } = 305 \; \frac{cm}{sec \; x \; amp}$$

Dividing Equation 24 by 26 we get,

$$V_{p\ max}/V_p = \frac{305}{50} \simeq 6 \qquad (27)$$

Equation 27 shows that when standing waves are used and the bed is located at a pressure minimum of the sound waves, we can get about six times the particle velocity as compared to traveling waves at the same current input to the voice coils. Thus, the difference in acoustic particle velocity and steady gas velocity is large in the case of standing waves, accounting for the higher values of collection efficiency.

E.   Compatibility of the Sonic Fluidized Bed Device with Automotive Systems

Experimental results in the preceeding section show that a sonic fluidized bed device can be used to clean automotive exhaust gases of their particulate matter by using standing sound waves. It is, however, imperative that the sonic flux be at least 0.5 watts/cm^2 to attain collection efficiencies in the order of 90%. Since sonic agglomeration has been demonstrated to be effective on particles from 0.05 μ to more than 8 μ in diameter, most of the range of particle sizes present in engine exhaust should be susceptible to this treatment. Since fluidized bed densities are generally 400 - 650 Kg/M^3, a 15 cm deep bed would have a pressure drop of approximately 5.9 cm of water. For a V-8 engine with a maximum exhaust of 95 standard liters/sec at 250°C the flow rate would be

$$95 \; x \; \frac{523}{273} = 182 \text{ liters/sec}$$

A 15 cm deep bed of 500 μ spheres can be kept fluidized at a velocity of approximately 300 cm/sec. Therefore, the bed would have to be approximately 607 cm^2 in cross-sectional area or 28 cm

in diameter. The bed can be fluidized in a relatively low range
of velocities. However, at lower exhaust rates retention times
would be longer and possibly enough coagulation could occur even
if the bed were not fluidized. Furthermore, at low gas
velocities the aerodynamic filtration efficiency of the bed
would increase because of the small distances between the bed
particles. Moreover, the fluidized bed device could be designed
to have a tapered cross-section, such that, a portion of the bed
would always fluidize at all flow rates.

The sound pressure levels in 5 cm diameter exhaust pipe
of an automobile vary from 160 to 170 dB, that is, 1 to 10
watts/cm^2. Assuming, an average value of 5.5 watts/cm^2, the
total sonic power in the exhaust pipe of an automobile is

$$5.5 \times \frac{\pi}{4} \times (5)^2 = 108 \text{ watts}$$

This magnitude of sound when spread over the cross-section of
a 28 cm diameter fluidized bed device would give a sonic flux
of 0.18 watts/cm^2, or approximately 1/3 of the sonic flux
(0.5 watts/cm^2) required for a 90% efficient device. Therefore,
the natural sound level in auto exhaust pipes is not sufficient
and an auxiliary acoustic unit would be needed to generate the
additional 200 watts of acoustic energy. One method of
accomplishing this desired result in an automotive application
is shown schematically in Figure 33.

As shown in Figure 33, the dirty exhaust gas would pass
through a relatively shallow fluidized bed. A sound generator
would be mounted above the bed, projecting the sound waves into
the bed. The submicron particles in the exhaust gas would
coagulate on the surface of the fluidized large particles under
the influence of the sonic vibrations.

Submicron particles once brought in contact with the course
material would adhere to it. Some attrition could be expected
but material dislodged from the large particles would be in the
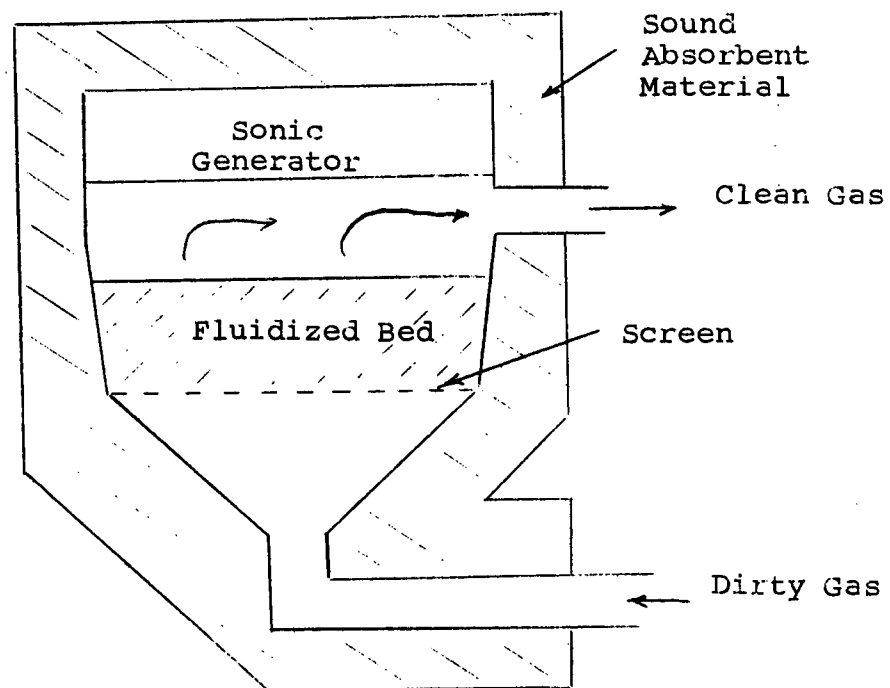form of large agglomerates, submicron particles once agglomerated

Figure 33

Sonic Agglomeration in a Fluidized Bed

require very high shearing forces to bring about deagglomeration. The agglomerated material dislodged from the bed could easily be separated with a state-of-the-art inertial separator such as a cyclone.

In the device envisioned there would be energy dissipation in the form of sonic vibrations. These will be within the audible range and consideration of sonic damping will be mandatory. Since we are relying on the high absorption and conversion of sonic energy by particulate beds into particle motion, it is anticipated that the damping will be achieved by adequate shielding with sound absorbant material which could even be particulate in nature.

The entire system would be expected to occupy less than one fifteenth cubic meters and weigh approximately 20 Kg with all the manifolding and sonic generator. The sonic generator would probably be an air driven siren which would be supplied by a belt driven air compressor.

An additional feature of this system is that the fluidized bed could well be chosen for its catalytic properties and aid in oxidizing unburned hydrocarbons and carbon monoxide.

It is difficult to estimate the cost of a workable device at this stage since no accurate design data exists, however, an educated guess would be somewhat less than $100 at the retail level.

Maintenance should be minimal. If the bed should "coke up" after long operation the bed could be dumped and refilled with approximately 10 Kg of a material which would probably cost no more than 20-30 cents per Kg, a cost of approximately $2.50.

V. CONCLUSIONS

The following conclusions are based on the results of our studies.

1. The thermal packed bed device has high collection efficiency (>95%) at gas-packing temperature differences exceeding 200°C.

2. Large gas-packing temperature differences in the bed can be maintained for a longer period of time with a high heat capacity packing material.

3. Collection efficiency of the thermal packed bed device does not change significantly with particle size and concentration in the range found in automobile exhausts.

4. Contamination buildup in the bed seems to have no significant affect on the collection efficiency of the bed at moderate gas velocities through the bed.

5. Increasing gas velocity from 15.5 to 130 cm/sec lowers the collection efficiency of the bed by only 10 to 15%.

6. Collection efficiency of the sonic fluidized bed device does not change appreciably with either the power input to the sound driver units or sound frequency when travelling waves are used.

7. Collection efficiency of the sonic fluidized bed device approaches 90% using standing sound waves at electrical power inputs to the sound driver units exceeding 125 watts.

8. Standing waves increase the aerosol particle velocity by a factor of 6 compared to travelling waves for the same power input to the sound driver units at a constant frequency.

From the above conclusions, it is evident that the thermal packed bed device can be employed to control particle emissions from spark ignition engines under most operating conditions.

The sonic fluidized bed device is capable of attaining collection efficiencies in excess of 90% with the use of standing waves and sound flux in excess of 0.5 watts/cm^2. The natural sound intensity in an automobile is of the order of 108 watts which is not sufficient when spread over the cross-sectional area of a 28 cm diameter bed needed to process automobile exhaust. Therefore, an auxiliary sound generator capable of supplying 200 watts of active acoustic power into the bed would be needed. This magnitude of auxiliary acoustic power and the corresponding sound absorbing mufflers would add both to the capital equipment and operating cost.

VI. RECOMMENDATIONS FOR FUTURE WORK

Further research should be carried out on the thermal packed bed device. The packed bed should be scaled up and optimized to process automobile exhausts under varying driving conditions with collection efficiencies close to that obtained with the laboratory model. Prototypes of the optimized device should be evaluated on test cars and further refinements made, if needed.

Moreover, it is necessary to have gas-packing temperature difference greater than 200°C for the device to have collection efficiency of 95% and greater. Techniques for cooling of the bed to obtain optimum gas-packing temperature difference need further development.

We are optimistic that the experimental data on the laboratory model can be used successfully to construct prototypes of the packed bed device for additional tests with exhausts from spark-ignition engines.

REFERENCES

1. "Particulate Lead Compounds in Automobile Exhaust Gas," Hirschler, D. A., et al, Ind. Eng. Chem., 49, 1131-1142 (1957).

2. "Concentration of Fine Particles and Lead in Car Exhausts," Mueller, P. K., et al, Symposium on Air Pollution Measurement Methods, ASTM Special Tech. Publication No. 352, 60-77 (1964).

3. "Automobile Exhaust Particulates -- Source and Variation," McKee, H. C. and McMahon, W. A., J. Air Pollution Control Assn., 10, 457-461 (1960).

4. "Nature of Lead in Automobile Exhaust Gas," Hirschler, D. A. and Gilbert, L. F., Archives of Environmental Health, Symposium on Lead, Feb. 1964.

5. "Characterization of Particulate Lead in Vehicle Exhaust-Experimental Techniques," Habibi, K., Environmental Sci. Tech., 4, No. 3, 239-248 (1970).

6. "Development of the Molten Carbonate Process to Remove Lead and Other Particulates from Spark Ignition Engine Exhausts," Natl. Air Poll. Control Admin., Contract No. CPA 70-3, Final Rept. by Atomic Intl., N. Amer. Rockwell, 1970.

7. "Studies on the Carcinogenicity of Gasoline Exhaust," Hoffman, D., et al, J. Air Poll. Control Assn., 15, 162-165, (1965).

8. "Blood Lead of Persons Living Near Freeways," Thomas, H. V., et al, Archives of Environmental Health, 15, 695-702, (1967).

9. "Lead in Soils and Plants -- Its Relationship to Traffic Volume and Proximity to Highways," Motto, H. L., et al, Environmental Sci. and Tech., 4, 231-237 (1970).

10. "Rotating Brush Aerosol Separator," Naval Air Systems Command, Contract No. N00019-68-C-0459, Final Rept. by IIT Res. Inst., 1969.

11. "Impaction of Dust and Smoke Particles on Surface and Body Collectors," Ranz, W. and Wong, J., Ind. Eng. Chem., 44, p. 1371 (1952).

12. Encyclopedia of Chemical Process Equipment, W. J. Mead, Editor, Reinhold Pub. Corp., N. Y., p. 731 (1964).

13. "Aerosols Consisting of Spherical Particles of Sodium Chloride," Matijevie, E., et al, J. Colloid Sci., 18, 91-93 (1963).

14. "Aerosol Studies by Light Scattering: IV - Preparation and Particle Size Distribution of Aerosols Consisting of Concentric Spheres," Espenscheid, W. F., et al, J. Coll. Sci., 20, 501 (1965).

15. "Particle Deposition from Turbulent Streams by Means of Thermal Force," Byers, R. L. and Calvert, S., AIChE, 63rd Natl. Meet., Preprint 27C, St. Louis, Feb., 1968.

16. "The Mechanis of Aerosols," Fuchs, N. A., the MacMillan Co., N. Y., 1964.

17. "On the Theory of Thermal Forces Acting on Aerosol Particles," Brock, J. R., J. Coll. Sci., 17, 768-780 (1962).

18. "Sonic Agglomeration of Carbon Black Aerosols," Stokes, C. A., Chem. Eng. Prog., 46, 423-432 (1950).

19. "Uber das Verhalten von Schwebstoffen in Schwingenden Gasen bei Schall -- Und Ultraschallfrequenzen," Brandt, O., Kolloid Zeit., 76, 272-278 (1936).

20. "Effect of the Magnitude of Acoustic Exposure on Acoustic Coagulation of Aerosols," Podoshevnikov, B. F., Zh. Prikl. Khimi, 34, 2664-2668 (1961).

21. "Acoustic Coagulation and Precipitation of Aerosols," Mednikov, E. P., Acad. of Sci., USSR Press, p. 118, 1963.

22. "Application of Sonic Energy in the Process Industries," Stokes, C. A. and Vivian, I. E., Chem. Eng. Prog. Symposium Series 1, 47(1), 11-21 (1951).

23. "Enhanced Deposition in an Aerosol Filter in the Presence of Low Frequency Sound," Beeckmans, J. M. and Keillor, S. A., J. Coll. Sci., 30, 387-390 (1969).

24. "Systematic Polarographic Metal Analysis," Lingane, J., J. Ind. and Eng. Chem., 15, 583-585 (1943).

25. "Polarographic Determination of Lead in Blood," Nylander, A. L. and Holmquist, C. E., AMA Arch. Ind. Hyg. and Occupational Health, 10, 183-191 (1954).

26. "Some Experiences with Polarographic Methods in Controlling a Lead Hazard in Brass Foundries," Weber, H. J., J. Ind. Hyg. and Toxicology, 29, 158-161 (1947).

27. "Methods for Determining Lead in Air and in Biological Materials," Amer. Pub. Health Assn., 2nd Ed., 38-39 (1955).

28. "A Polarographic Method for Lead and Zinc in Paints," Abraham, M. B. and Huffman, R. S., Ind. and Eng. Chem., 12, 656-666 (1940).

29. "Official Methods of Analysis of the Association of Official Agricultural Chemists," Assn. of Official Agricultural Chemists, Washington, D. C., 10th ed., 367-74 (1965).

30. "Colorimetric Determination of Traces of Metals, Vol. III," Sandell, E. B., 563-571, Inter Science Publishers, Inc., N. Y., 1959.

APPENDIX A

ANALYTICAL TECHNIQUES

ANALYTICAL TECHNIQUES

The following analytical techniques were used in this study:

1. Reflectometer

Initially, when carbon particles were used as the test aerosol, a reflectometer was used to determine the collection efficiency of the thermal bed. Aerosol was sampled both upstream and downstream of the packed bed on white fiberglass filters. The reflectivity of the filters was measured using a reflectometer. If it is assumed that the amount of light reflected from the filter follows Beer-Lambert Law, then

$$\frac{I}{I_0} = \exp{(-AC)} \qquad\qquad (1\text{-}A)$$

where I is the transmitted or reflected light, I_0 is the incident light, A is a constant, and C is the concentration of light absorbing particles.

$$\ln{\frac{I_1}{I_0}} = -AC_1 \qquad\qquad (2\text{-}A)$$

and

$$\ln{\frac{I_2}{I_0}} = -AC_2 \qquad\qquad (3\text{-}A)$$

where the subscripts 1 and 2 refer to the upstream and downstream samples, respectively. From Equations 2-A and 3-A an expression for percent collection efficiency, E, was derived.

$$E = \frac{C_1 - C_2}{C_1} \times 100 = \frac{\ln(I_1/I_0) - \ln(I_2/I_0)}{\ln(I_1/I_0)} \times 100 \qquad (4\text{-}A)$$

Equation 4-A has been used to calculate the collection efficiency of the thermal packed bed device from the reflectometer readings.

2.   Polarographic Technique

Polarographic techniques have been used widely to determine microgram quantities of lead (Refs. 24, 25, 26, 27, 28). The polarograph is a device that produces a diffusion current which is proportional to the lead ion concentration in a supporting electrolyte. The following technique was used to calculate lead chloride concentration in the aerosol stream using a Sargent Model XXI Polarograph.* The polarograph was calibrated using standard solutions of $PbCl_2$ to get the calibration curve shown in Figure 34.

Aerosol samples, both up- and downstream of the packed bed, were collected on Gelman type A glass fiber filters. The filters were placed in 100 ml beakers and boiled with distilled water for 1 hr. The liquid was allowed to concentrate to about 15 ml and then the samples were cooled to room temperature. The concentrated mother liquor was washed into a graduated cylinder and diluted to the 25 ml mark. The entire contents of the cylinder were poured into the polarographic cell and 10 ml of supporting electrolyte was added. The supporting electrolyte consisted of 0.1 M KCl and 0.01% gelatin. The cell was purged with a stream of dry, high purity, nitrogen for 10 min to remove the dissolved oxygen. After purging, the cell was sealed to prevent air from entering the cell. Mercury drops from the dropping mercury electrode were allowed to enter the cell containing the

---

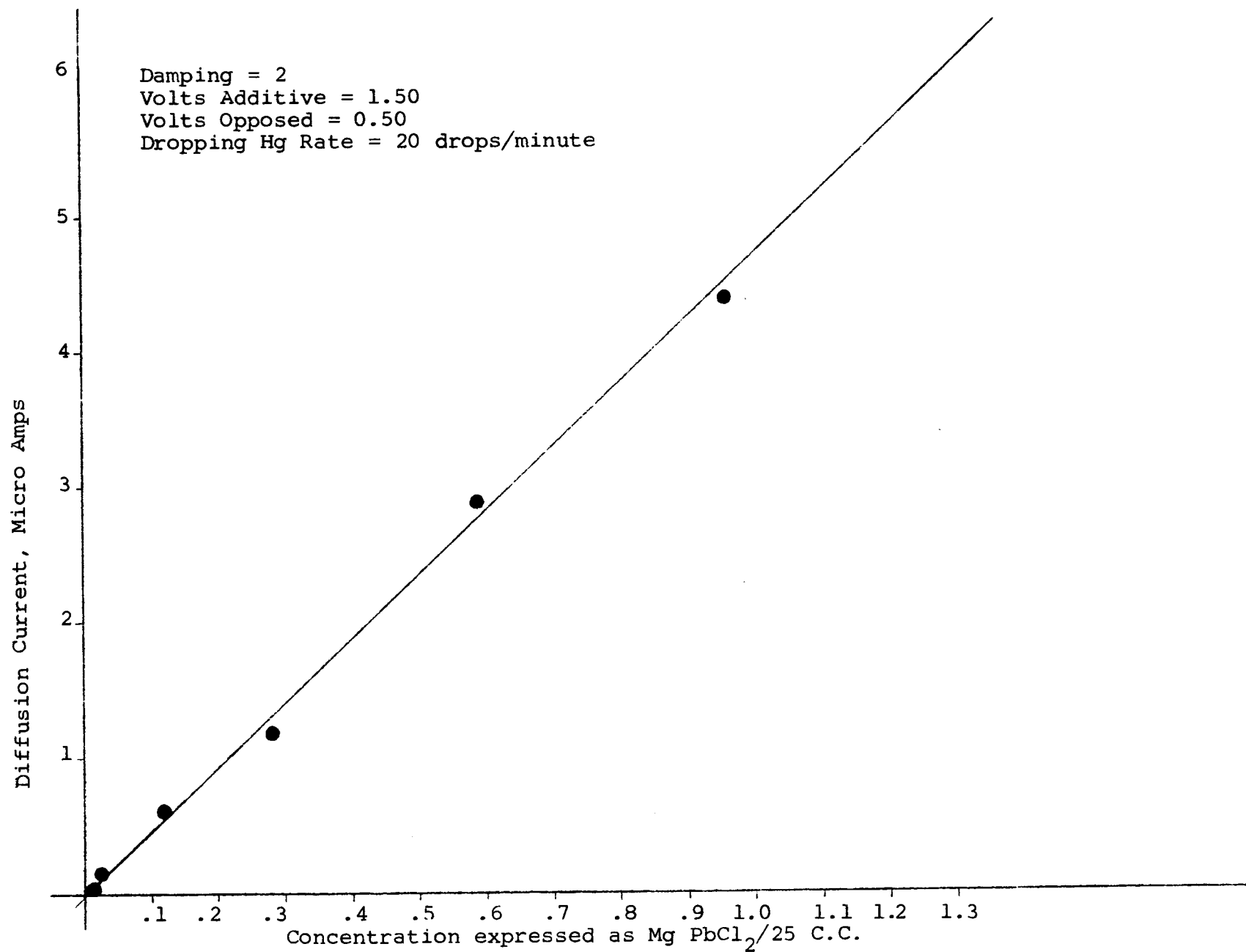*Manufactured by E. H. Sargent & Co., Chicago, Illinois.

Figure 34 : Calibration Curve for the Polarograph

solution at the rate of one drop every 3 sec. The diffusion current corresponding to lead ions was determined from the polarographic trace and the corresponding $PbCl_2$ concentration obtained from the calibration curve on Figure 34. The $PbCl_2$ concentration was then calculated from the aerosol sampling rate, sampling time, and the polarograph results.

While the polarograph method is accurate, it does not lend itself to rapid analysis of a large number of samples. An alternate time saving and just as accurate colorometric method described in Section 3 was used to analyze samples after the month of July.

3. Colorimetric Technique

The colorimetric method using dithizone permits detection and measurement of lead concentration as low as 0.1 μt lead with sufficient accuracy (Ref. 29).

The following procedure was used to analyze filter samples in the present study. Immediately after conducting a test run, upstream and downstream filter samples were placed in small wide-mouth jars. The jars were sealed to eliminate any lead con- tamination of the filters. The filters were removed from the jars and placed in 150 ml beakers. The beakers were then heated with 100 ml of 1% nitric acid solution in water to extract the lead from the filter papers. The heating was done at 80 °C for 1 hr to ensure total dissolution of $PbCl_2$ particles. The beakers were cooled to room temperature and the samples were filtered into 200 ml volumeteric flasks through Millipore membrane with pore opening of 0.45 μ. The filter and beaker were rinsed with 1% nitric acid and the total volume of the filtrate was brought up to 200 ml mark with addition of 1% acid solution. The reagents were prepared by Sandell's tech- nique (Ref. 30) as follows:
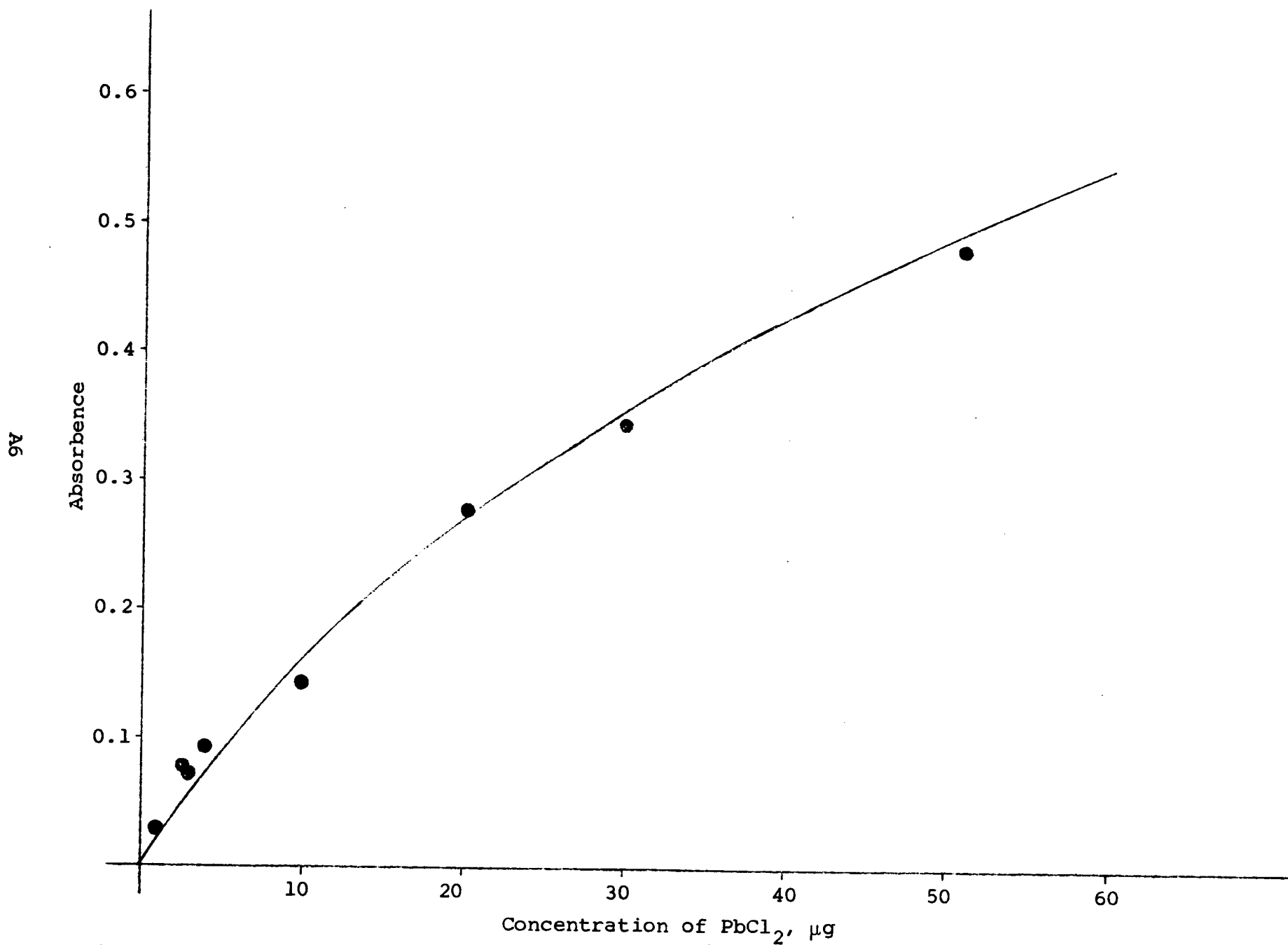
Figure 35- Calibration Curve for Lead Chloride vs Absorbence at Wavelength of 520 mμ

Dithizone: Reagent grade.
                  Stock solution, 0.005% in CCl_4.*
                  Solution for analysis prepared by diluting stock
                  to 0.001% at the time of analysis.

Buffer: NH_3-CN-SO_2 solution
                  to 98 ml of concentrated reagent NH_4OH were added
                     0.75 g of KCN and 0.375 g NA_2SO_3. The mixture
                  was diluted to a final volume of 250 cc.

Analysis
Wavelength: 520 mμ.

Procedure: Add 10 ml of 0.001% dithizone to 10 ml of the
                  buffer in a 60 ml separatory funnel. An appropri-
                  ate size aliquot (usually 2 cc) of $PbCl_2$ extract
                  is added next. The mixture is extracted for
                  1 min. The CCl_4 layer is immediately drawn off
                  into the colorimetric tube for analysis with a
                  Spectronic 20 spectrometer.**

     The absorbance given by the spectrometer is a measure of
lead concentration in the solution. A calibration curve shown
in Figure 35 was prepared using standard solutions of lead
chloride. The aerosol concentration was easily calculated from
the calibration curve and the volume of aerosol sampled.

---

*Dithizone is unstable and must be kept in a refrigerator until
  diluted for the day's analysis.

**Manufactured by Beckman Instruments.

DISTRIBUTION LIST

Copy No.	Recipient
1 - 100	National Air Pollution Control Administration Consumer Protection & Environmental Health Service Division of Motor Vehicle R & D 5 Research Drive Ann Arbor, Michigan 48103 Attn: Mr. Charles Gray, Project Officer
101	Division of General Services Environmental Health Service, PHS Parklawn Building, Room 4A-44 5600 Fishers Lane Rockville, Maryland 20852 Attn: Martin K. Trusty, Contracting Officer Negotiated Contracts Section
102	IIT Research Institute M.J. Klein/Division Files
103	IIT Research Institute S.L. Blum
104	IIT Research Institute G.E. Burkholder/Main Files
105	IIT Research Institute R. Karuhn
106-110	IIT Research Institute S.K. Sood
111	IIT Research Institute J.D. Stockham/Section Files
112	IIT Research Institute P. Caputo